Structural, Morphological, Optical, Luminescent and Magnetic Properties of Nanostructured ZnO Thin Film

Visweswaran S (visudharan@gmail.com)
Annamalai University https://orcid.org/0000-0002-9631-7496
R. Venkatachalapathy
Annamalai University
M. Haris
Karunya Institute of Technology and Sciences
R. Murugesan
Thiru Kolanjiappar Government Arts College

Research Article

Keywords: ZnO thin film, substrate temperature, highly transparent, weak ferromagnetic behavior

Posted Date: March 1st, 2021

DOI: https://doi.org/10.21203/rs.3.rs-243700/v1

Structural, Morphological, Optical, Luminescent and Magnetic properties of nanostructured ZnO Thin Film

S.Visweswaran [1,*], R.Venkatachalapathy [1], M.Haris [2], R.Murugesan [3]

[1] Department of Physics, Annamalai University, Chidambaram, Tamilnadu – 608 002
[2] Department of Physics, Karunya Institute of Technology and Sciences, Coimbatore – 641114Tamilnadu
[3] PG and Research Department of Physics, Thiru Kolanjiappar Government Arts College, Vridhachallam – 606001, Tamilnadu

Corresponding author email id: visudharan@gmail.com

Abstract

ZnO thin film deposited on the glass substrate at various substrate temperature by spray technique using perfume atomizer. The deposited ZnO thin films are annealed at 450ºC. The deposited films are highly transparent and adhered to the substrate. The structure and microstructural, morphological, compositional, optical and luminescent characteristics were studied by X-ray diffraction (XRD), Raman, Field emission scanning electron microscope (FE-SEM with EDX), Atomic force microscope (AFM), Ultra violet visible spectrophotometer (UV-Vis) and photoluminescence spectroscopic techniques. The crystalline nature of annealed film were confirmed from XRD and the shows preferred orientation along (1 0 1) plane. At higher substrate temperature, reorientation of planes was seen. The spherical shaped grains are observed from morphological studies. The roughness of ZnO film, one of the key parameter obtained from AFM, increases with substrate temperature. The high transparency of about 80% in visible region are obtained for ZnO film with band gap ranging from 3.24 – 3.19 eV. The presence of defects in ZnO films are identified from PL bands. The electronic vibrations in ZnO film were understood from Raman spectra. The weak ferromagnetic behavior at room temperature is

observed and exchange interactions stemming from oxygen vacancy produce BMP and subject to RTFM in ZnO.

Keywords: ZnO thin film, substrate temperature, highly transparent, weak ferromagnetic behavior.

1.1 Introduction

ZnO belonging to II – VI element, is a compound semiconductor. Its energy band gap is 3.37 eV and it possesses large exciton binding energy. The ZnO crystallizes in three forms a. zinc blende, b. rock salt, and c. wurtzite. The stable ZnO phase (hexagonal wurtzite) is obtained thermodynamically at room temperature, where each Zn^{2+} ions are surrounded by four O^{2-} at the corners of the tetragon. The ZnO based TCO film is known for its exceptional performance, so it is used in variety of industrial and medicare applications such as piezoelectric and pyroelectric properties [1], surface acoustive wave devices (SAW), biosensors, drug delivery, anti microbial and antifungal activity, spintronics and optoelectronic devices [2], solar cells [3], photodetector and photovoltaics, photoelectrochemical water splitting [4], photocatalytic [5], gas sensor [6]. The ZnO films were grown from inorganic and organic precursors such as nitrates, chlorides, perchlorates, acetates and acetylacetonates respectively were reported by number of authors [7]. The ripple like morphology is obtained for spin coated ZnO film, cubic like structures is noticed for the spin coated ZnO by solution growth at various time interval and flakes like formation is seen for ZnO film doped with Al is reported [8]. T. Srinivasulu et.al, investigated the influence of Fe doped ZnO film by spray pyrolysis. No structural deformation is observed for the Fe doped ZnO film. Also, ZnO film shows the paramagnetic behavior in pure form and ferromagnetic for Fe doped film [9]. The microstructures of ZnO thin film such as spindle like, rod, hexagonal

plate like morphologies at different molar concentration are investigated [10]. The ZnO film obtained with *c // n* and *a // n* orientation reported by L.Znaidi.et.al [11]. Ahamed et al. investigated the optical and structural properties of B doped ZnO nanostructures by sol gel technique. The preferred orientation of (002) plane vanished for B doped ZnO. The grain size increased with the dopant concentration and the irregularity in film's morphology. The ZnO film achieved 90% transmittance in visible region decreases with dopant concentration. The Eg of ZnO film decreases as the grain size increases [12]. Alsaad et al, fabricated transparent ZnO thin film whose transmittance ($\lambda > 70\%$) in the visible region and the transmittance of (B, Al, Ga, In) doped ZnO thin film is in close proximity with undoped ZnO film. The decrease in the optical energy gap of the doped ZnO thin film is due to the variation in crystallite size. The XRD patterns demonstrate a large difference in angular positions between the undoped and group III elements doped ZnO thin films [13]. Mn doped ZnO thin film coated on glass substrate by spray pyrolysis technique. The stoichiometry of the film at 450ºC was confirmed by RBS spectra and found to depend on the substrate temperature. By doping Mn in ZnO, the wurtzite hexagonal structure remains unchanged. The maximum transmittance 100% was obtained for ZnO thin film at 500ºC, resulting in decrease in optical scattering. The bandgap energy values are 3.22eV, 3.24eV and 3.27eV respectively for the films at 400ºC, 450ºC and 500ºC. The doping of Mn has no effects on the resistivity ZnO and Mn doped ZnO thin film [14]. Here we present the impact of substrate temperature on the structural, morphological, optical and magnetic properties of perfume spray deposited ZnO thin film.

2 Experimental details

ZnO thin films were fabricated by spray technique using a perfume atomizer as reported [15,16]. The commercially available glass substrates (75 x 25 mm) (Blue star Micro glass slides) were used for film deposition. The glass substrate was cleaned and degreased using distilled.water, HCL and acetone and dried. 0.1 M of Zinc acetate dihydrate, AR grade (SRL chemicals) is diluted with deionized water and ethanol in proportion 2:1. The solution is dispersed ultrasonically for its homogeneity and transparency for about 30 minutes. The solution was then sprayed onto the preheated glass substrate glass substrate maintained at 300ºC, 350ºC, 400ºC and 450ºC and is dried. Finally all the deposited films were annealed in a muffle furnace at 450ºC for 2 hrs under air atmosphere. The resultant ZnO thin films are well adherent to the substrate.

2.1 Characterization techniques

The crystallographic structure of ZnO thin film was studied by PANalytical/ Xpert3 powder X-ray diffraction (XRD) instrument. The surface morphology of ZnO films were studied by FE-SEM (zeiss, Bruker instrument) and Atomic force microscope (Agilent 5500). Ultra-violet visible (UV-Vis) absorbance and transmittance measurements were conducted on UV-visible spectrophotometer (Thermofisher 220 instrument). Photoluminescence (PL) measurements were performed by Varian Cary Eclipse PL analyser. Room temperature Raman studies were conducted by micro Raman spectrometer SEKI, Japan. The magnetization (M) against applied field (H) at room temperature was evaluated using Lake Shore, vibrating sample magnetometer (VSM).

3 Results and Discussion

3.1 Structural characterization

The XRD patterns of ZnO thin film deposited at various substrate temperatures and annealed at 450 °C were recorded over the 2θ range from 10° – 80°. Fig.1 displayed the polycrystalline nature of the film, showing multiple peaks and indexed to the standard JCPDS card 89-1397, corresponding to hexagonal wurtzite structure. It belongs to $P6_3mc$ space group. The high crystallinity of ZnO thin film is indexed by the presence of narrow and sharp reflection peaks [17]. The peaks at angle 2θ around 31.7º, 34.24º, 36.19º, 47º, 56°, 62º, 66°, 67º corresponds to (100), (002), (101), (102), (110), (103), (200), and (112) reflection planes. There are three prominent planes (100), (002), (101) at 2θ, 31.7º, 34.24º, 36.19º and the weak reflection planes (102), (110), (103), (200), (112) and (201) at 2θ around 47º, 56°, 62º, 66°, 67º are observed. No peak other than ZnO is observed within the detection limit. The as deposited and annealed ZnO thin films shown similar XRD pattern with intensity variation. The analogous results were reported by researchers [18, 19]. The annealing resulted in better crystallinity and the oxidation of ZnO thin film fabricated at 300ºC [20]. The observed variation in the peak intensity with the substrate temperature is due to different film thickness [21]. Further at 450°C, the degree of crystallinity is deteriorated and the reflection of (002) plane is more pronounced confirmed the orientation along *c* - axis perpendicular to the substrate [22, 23] and this may lead to the granular structure of the film [24]. Hence, the reorientation of planes at 450°C is due to the lowest surface energy of the plane and internal stress at this temperature [25, 26]. Nitu kumara et al, reported the decrease in the intensity of ZnO thin film at higher substrate temperature. The decreasing trend was due to the incomplete conversion of Zinc precursor to ZnO [27]

The XRD parameter such as crystallite size (D), lattice strain (ε) and dislocation density (δ) is found to decrease with substrate temperature. The decrease in the value of dislocation density (δ)

implies the film has few lattice defects. The structural parameters, crystallite size (D), d-spacing, stress and strain, dislocation density (δ), volume of unit cell (V), SSA are summarized in table 1.

The lattice parameters are evaluated using the following relation

$$a = \frac{\lambda}{\sqrt{3}sin\theta};\ c = \frac{\lambda}{sin\theta}$$

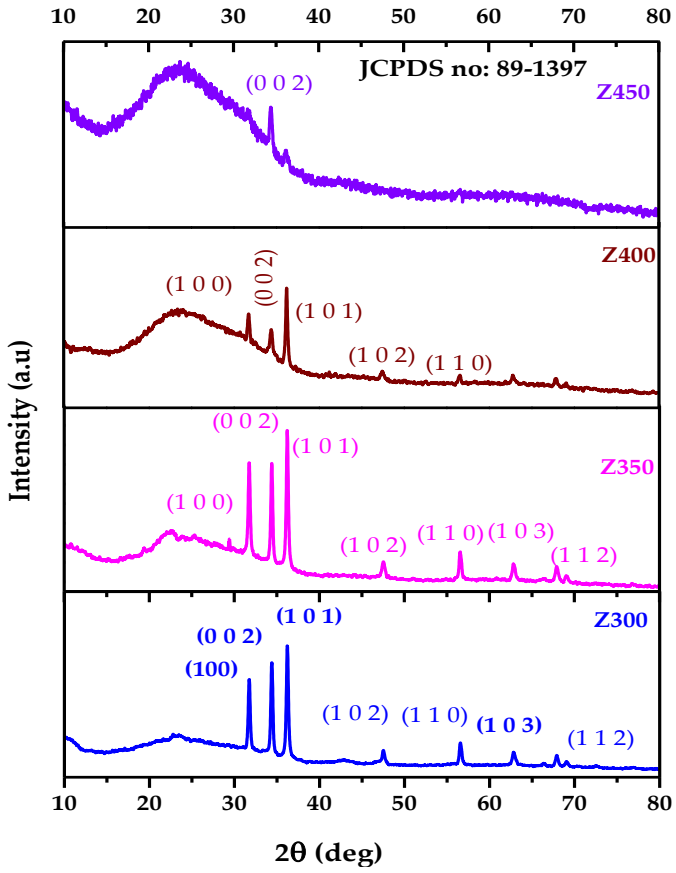

Fig 1. XRD patterns of annealed ZnO thin film at different substrate temperature

The lattice strain (ε) and the stress (σ) in the film is calculated using the expression

$$\varepsilon = \frac{c - c_0}{c_0} \text{ x } 100\%$$

$$\sigma = -4.5 \text{ x } 10^{11} * \varepsilon$$

The unit cell volume (V) was estimated from

$$V = \frac{\sqrt{3}}{2} a^2 c$$

The crystallite size of (101) plane at substrate temperature 300ºC, 350ºC, and 400ºC are estimated as 48.96 nm, 40.61 nm and 35.66 nm respectively and the crystallite size of (002) plane at 450ºC is 24.14 nm expressing the microstructural character of deposited ZnO film. The crystallite size (D) of intense (101) plane is found to decrease with substrate temperature. Likewise the full width half maximum (β) decreases with substrate temperature. The higher the crystallite size (D), lower the dislocation density (δ) [28]. The negative sign in stress values represents the compressive stress in ZnO thin films. The variation in lattice parameter 'a' and 'c' are related to a_0 and c_0 [29].

Table:1 XRD parameters FWHM, crystallite size (D), strain , stress , d-spacing, lattice constant a and c and volume of unit cell, specific surface area.

Substrate temperature (deg)	2θ (deg)	(hkl) plane	Crystallite Size D (nm)	Dislocation density $\delta \times 10^{-14}$ l/m^2	Strain	Stress x 10^{10} Nm^{-2}	d-spacing (Å)	a (Å)	c (Å)	V $(Å)^3$	SSA
300	36.25	101	48.96	4.171	-0.0491	2.209	2.476	2.858	4.950	35.014	21.663
350	36.08	101	40.61	6.063	-0.0449	2.020	2.479	2.871	4.972	35.490	26.117
400	36.08	101	35.66	7.863	-0.0449	2.020	2.483	2.871	4.972	35.490	29.742
450	34.36	002	24.14	17.160	0.0013	-0.058	2.608	3.010	5.213	40.901	43.936

3.2 FESEM analysis

The surface microstructures of ZnO thin films at different magnifications are displayed in Fig 2 (a-h). The increase in substrate temperature and annealing has influenced ZnO thin film. The ZnO film showing different morphology at various substrate temperatures and random orientation are obtained [30]. Fig.2 (a,c,e) showed the wrinkled shaped fibrous structure with porous, spherical granules are randomly distributed over uniformly layer of ZnO thin film deposited at 300°C, 350°C and 400°C which is due to the influence of temperature between first layer and the other layer of the ZnO [22]. The fibrous structure formation is due to slow cooling. During cooling, the ions may have sufficient time to aggregate along crystal planes with similar lattice match. This fibrous like morphologies have large surface area shown in Table:1, that it may be used for optoelectronic devices and photovoltaic devices application [24]. Some voids are observed in between the nanostructures through which oxygen and water molecule propagates into the ZnO thin film [31-33]. The energy gained due to annealing merge the grain boundaries with each other forming larger grains [34].The fiber like morphology switched to the surface having spherical shaped grains with high inter grain spacing at higher substrate temperature 450°C [15, 35]. The uniform distribution of spherical grains can be obtained using acetate precursor as reported by Harish Bahadur et.al. [36].

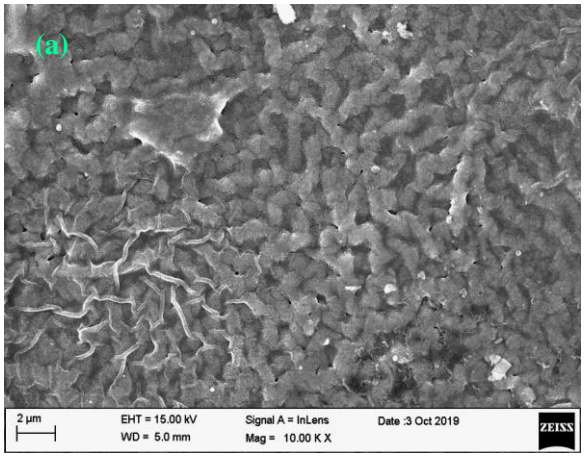
(a)
2 µm
EHT = 15.00 kV
WD = 5.0 mm
Signal A = InLens
Mag = 10.00 K X
Date :3 Oct 2019
ZEISS

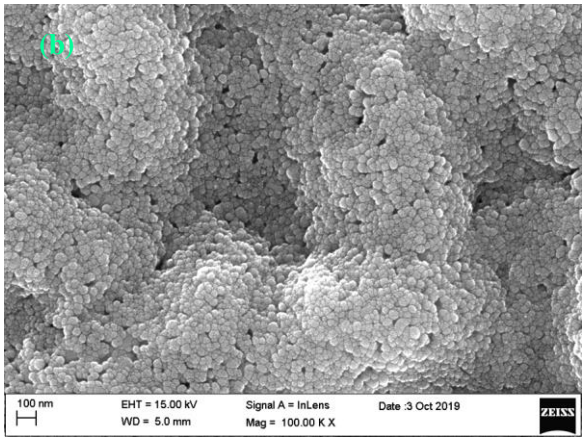
(b)
100 nm
EHT = 15.00 kV
WD = 5.0 mm
Signal A = InLens
Mag = 100.00 K X
Date :3 Oct 2019
ZEISS

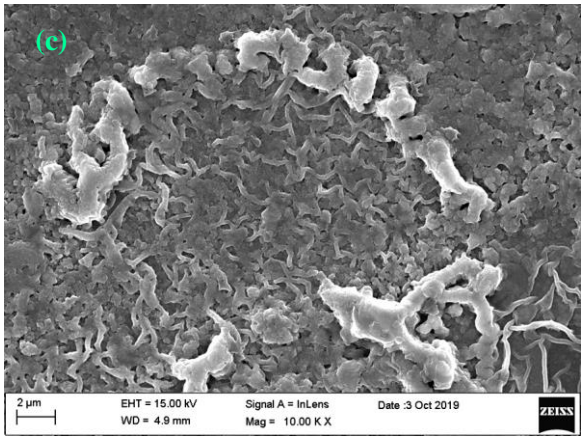
(c)
2 µm
EHT = 15.00 kV
WD = 4.9 mm
Signal A = InLens
Mag = 10.00 K X
Date :3 Oct 2019
ZEISS

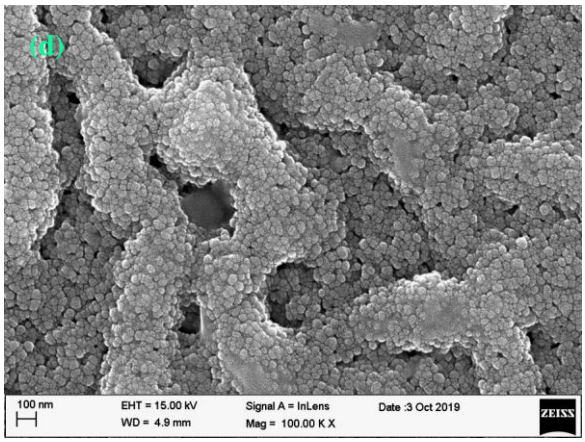
(d)
100 nm
EHT = 15.00 kV
WD = 4.9 mm
Signal A = InLens
Mag = 100.00 K X
Date :3 Oct 2019
ZEISS

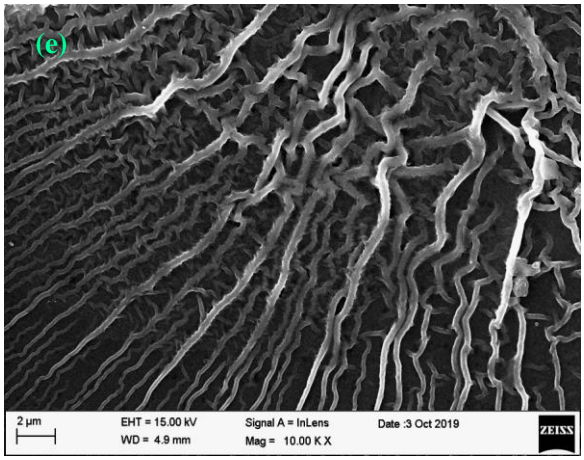
(e)
2 µm
EHT = 15.00 kV
WD = 4.9 mm
Signal A = InLens
Mag = 10.00 K X
Date :3 Oct 2019
ZEISS

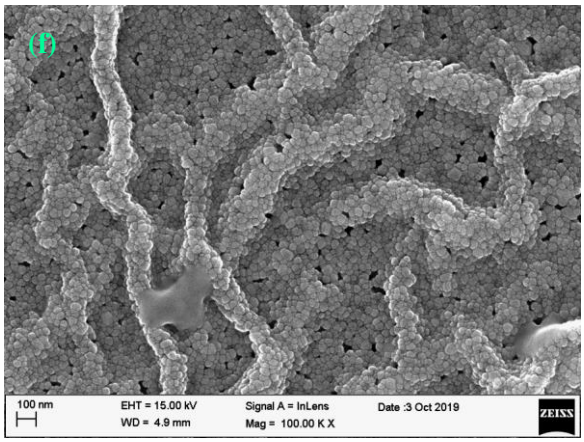
(f)
100 nm
EHT = 15.00 kV
WD = 4.9 mm
Signal A = InLens
Mag = 100.00 K X
Date :3 Oct 2019
ZEISS

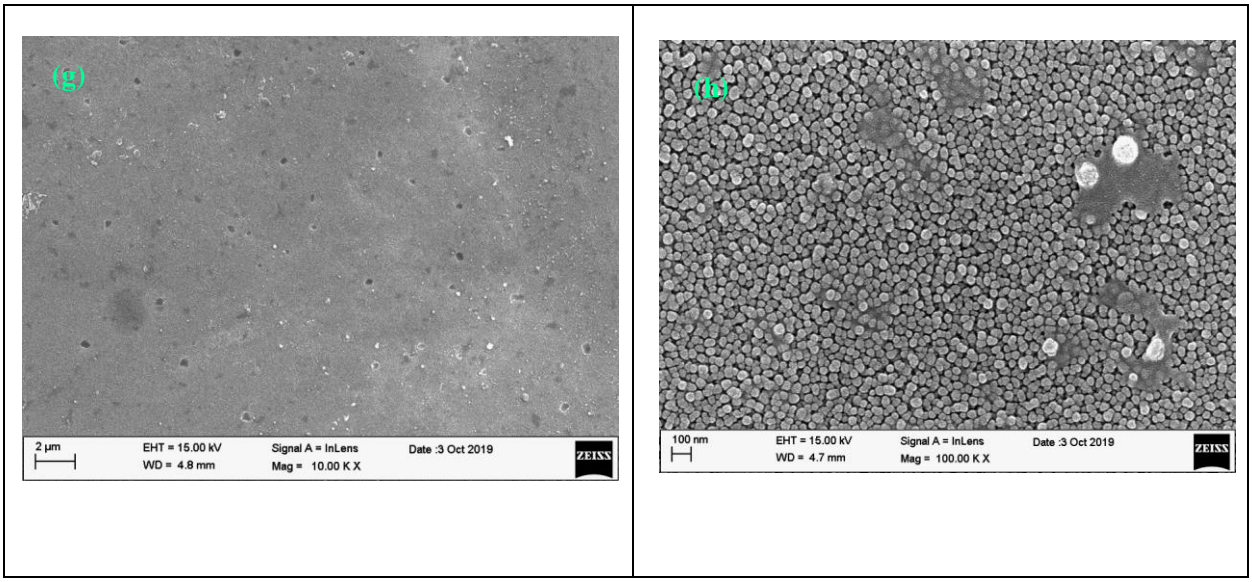

Fig. 2 FE-SEM images of ZnO thin films at substrate temperature (a,b) 300ºC, (c,d) 350ºC, (e,f) 400ºC and (g,h) 450ºC

3.3 EDS micro elemental analysis

Fig. 3(b,d,f,h) shows EDS spectra of ZnO thin film at different substrate temperatures and the presence of Zn and O is confirmed. The EDS results depicts that none of the samples are well stoichiometric. The Zn distribution (%) in the grown structure decreases with substrate temperature might be due to the lower density of nucleated ZnO. And as a result increasing trend in O (%) is ascribed to the oxygen incorporation during spray deposition [37, 38].

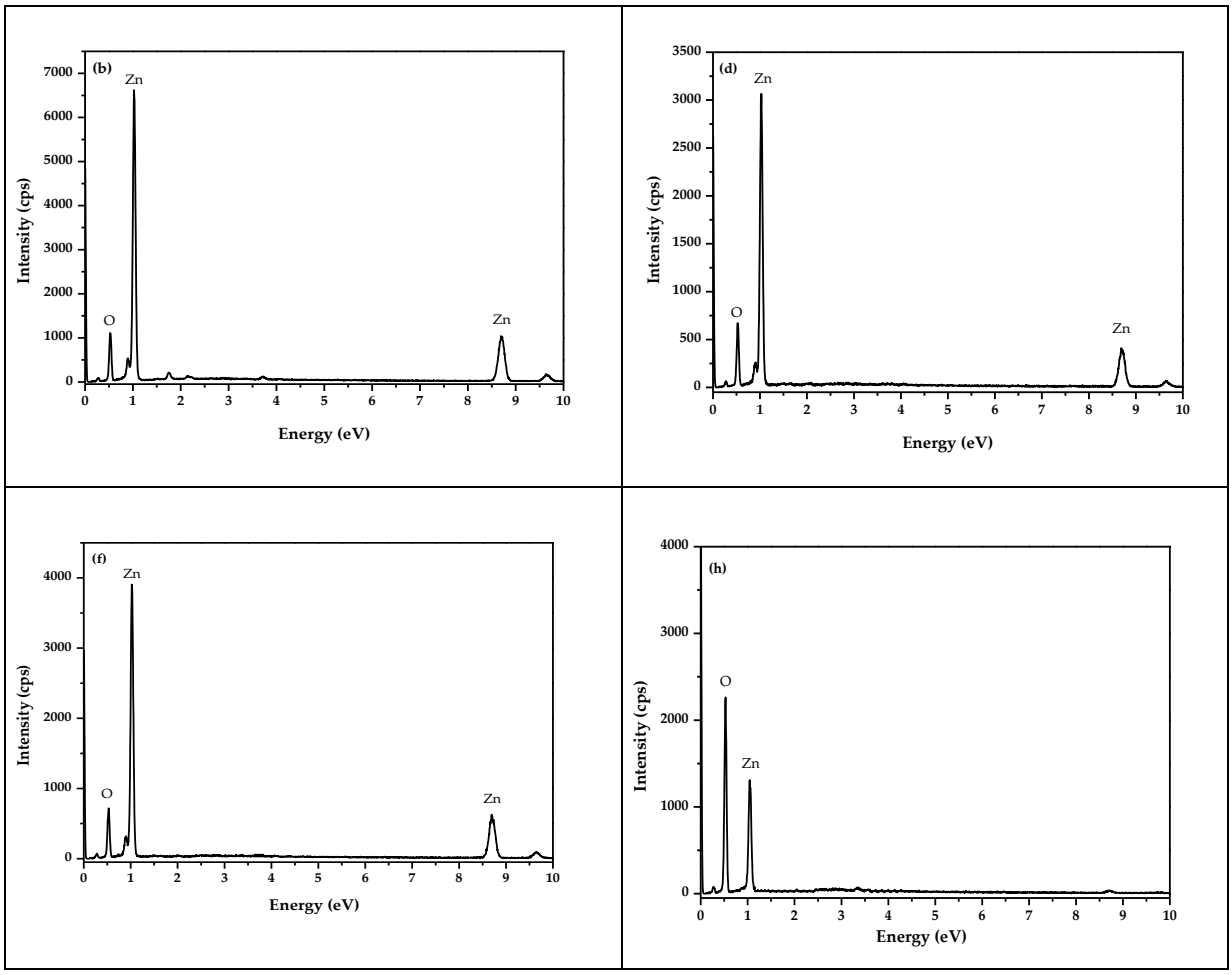

Fig. 3 EDS spectra of ZnO film at substrate temperatures

3.4 AFM Analysis

The surface microstructure of ZnO film deposited on glass substrate at various substrate temperatures are analyzed from AFM measurements. The Fig. 4 (a – h), depicts the 2D and 3D profile images of ZnO thin film. The micro structural images are on par with the FE-SEM morphologies. The surface roughness is minimum and maximum for the film at lower (300ºC) and higher substrate temperature (450°C). At temperatures between 300°C and 450ºC, the different surface morphologies like wrinkle shaped and spherical grains are obtained. Fig. 4(c)

illustrates columnar shaped grains perpendicular to the substrate surface showing wrinked appearance [39].

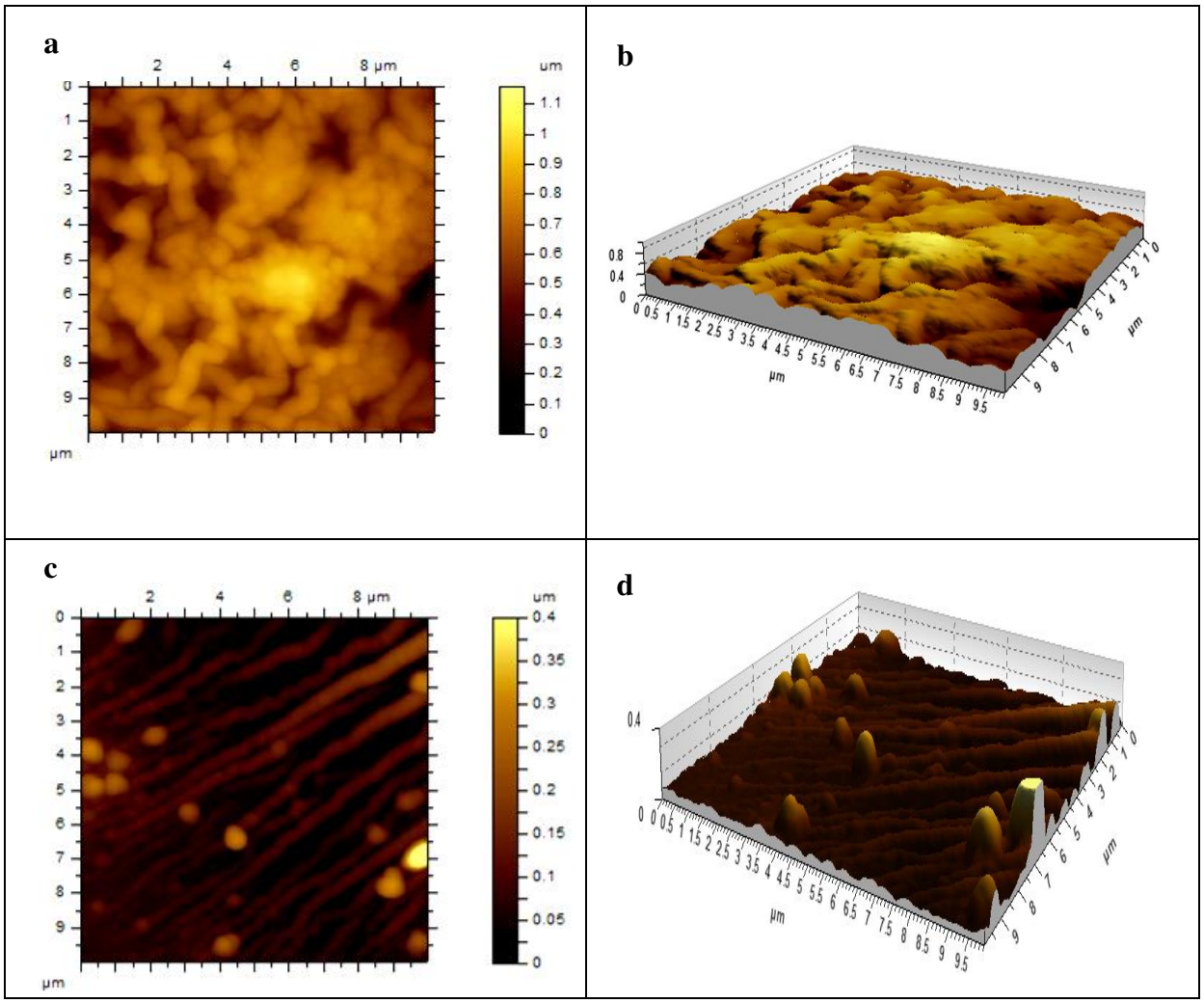

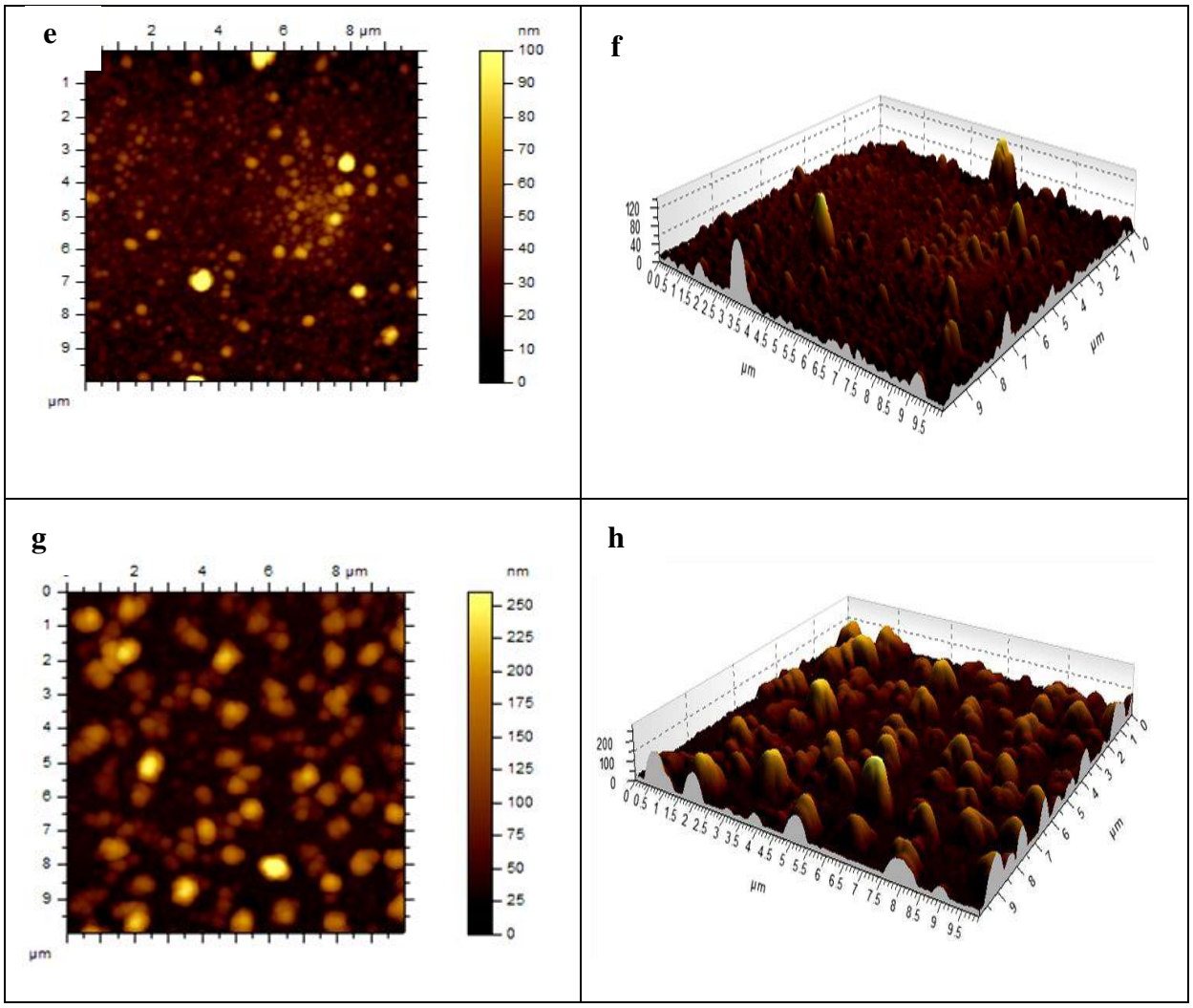

Fig. 4 (a - h), 2D and 3D AFM image of ZnO thin film at different substrate temperatures.

3.5 Optical characterization

The UV-Vis absorbance and transmittance spectra of ZnO film deposited at different substrate temperature were recorded over wavelength range 200 – 1100 nm, is displayed in Fig.5. The presence of two absorption peaks at around 316 nm and 360 nm for all the film are identified. The absorption peak around 316 nm refers to the excitonic absorption. This excitonic absorption peak lies significantly below the 360 nm *i.e*, the band gap of ZnO, is associated with the quality

of nanoparticle distribution [40]. The strong absorption peak around 360 nm is the characteristic of ZnO film. All the films shows high optical transparency of $\geq$ 80% in visible region, which is one of the prime requirement for device applications such as optoelectronic and solar cell application and low transparency in the UV region. The high transmittance of ZnO thin film emphasize that the film is neither absorbed nor scattered the light [41]. The absence of interference fringes in the transmittance spectra is correlated to diffusion phenomena and small grain size of the deposited films [9, 42].

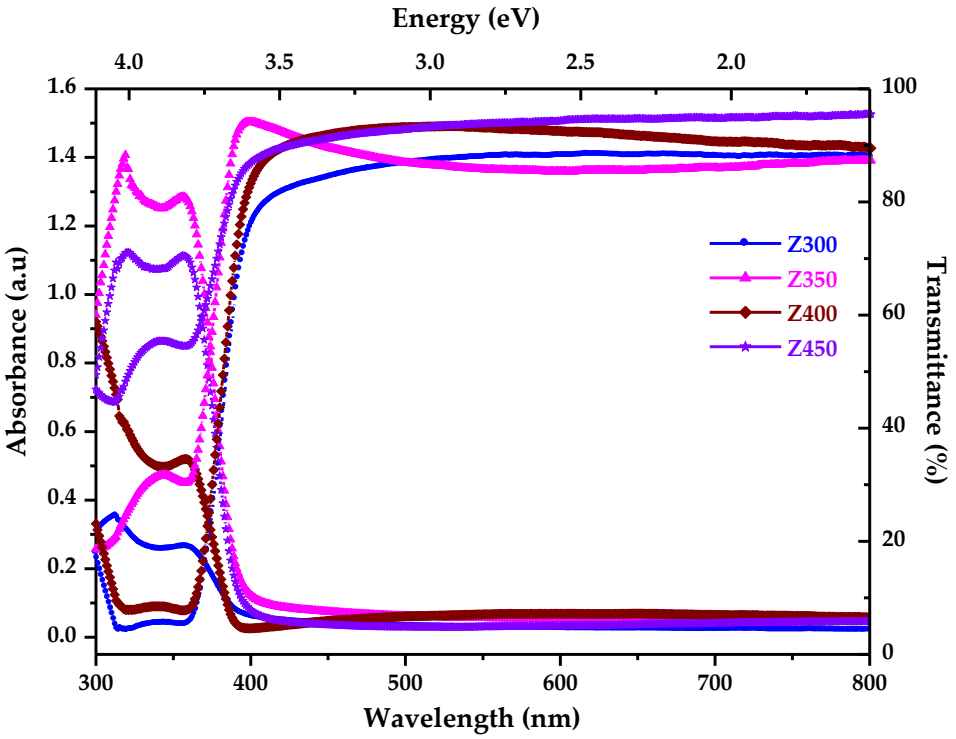

Fig.5 UV Vis absorbance and transmittance spectra of ZnO thin film

The transmittance drops appreciably around 370 nm in UV region and it is the intrinsic band gap of ZnO film (3.3 eV). The shift in absorption edge towards lower wavelength regime for the film deposited at various substrate temperatures is displayed. It is observed for all the film, the transmittance decreases below 400 nm, is due to the fundamental absorption edge attributed to

the electron, that makes cross over from valance band to conduction band. The change in optical transmittance of the film is related to surface roughness and the virtue of crystallinity of ZnO film [9]. The blue shift is identified for the ZnO film deposited at 450°C and hence the particle is confined to the quantum level. Generally, the quantum size effect occurs for the particles upto 8 nm [43, 44] and in our case, the crystallite size of the ZnO film is above the expected quantum confined size.

The relation used for manipulating the absorption coefficient is given by the formula,

$$\alpha = \frac{2.303}{t} A = \frac{1}{t} ln \frac{1}{T}$$

where d is the thickness of the film, A and T are the absorbance and transmittance of the film deposited. The absorption coefficient of ZnO film is displayed in the Fig: 6. The absorption coefficient varies exponentially with incident photon energy near absorption edge and obeys urbach relation [41].

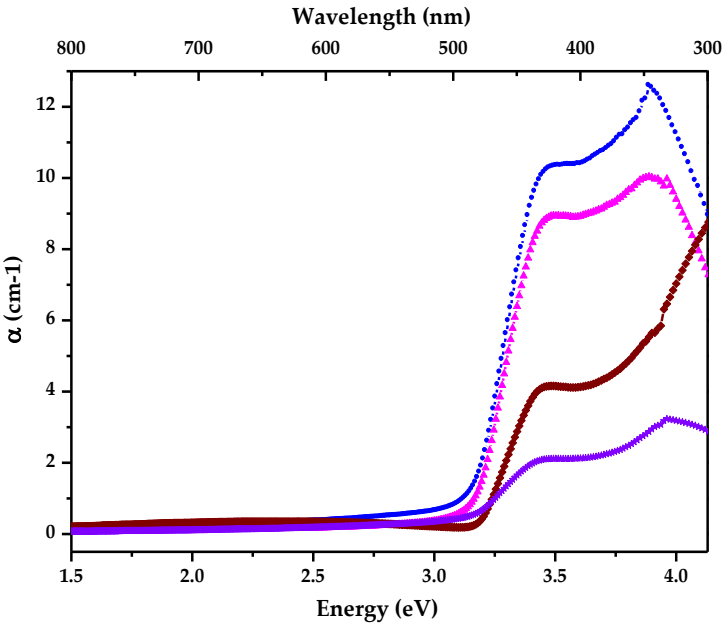

Fig 6. Absorption coefficient Vs Wavelength plot of ZnO film

The band gap for ZnO film estimated from the Tauc's plot is displayed in Fig 7.

The optical band gap E_g was estimated from the relation

$$(\alpha h\nu)^2 = A(h\nu - E_g)$$

where 'A' is the proportionality constant, 'E_g' is the direct band gap, 'hν' is the incident photon energy and 'α' is the absorption coefficient.

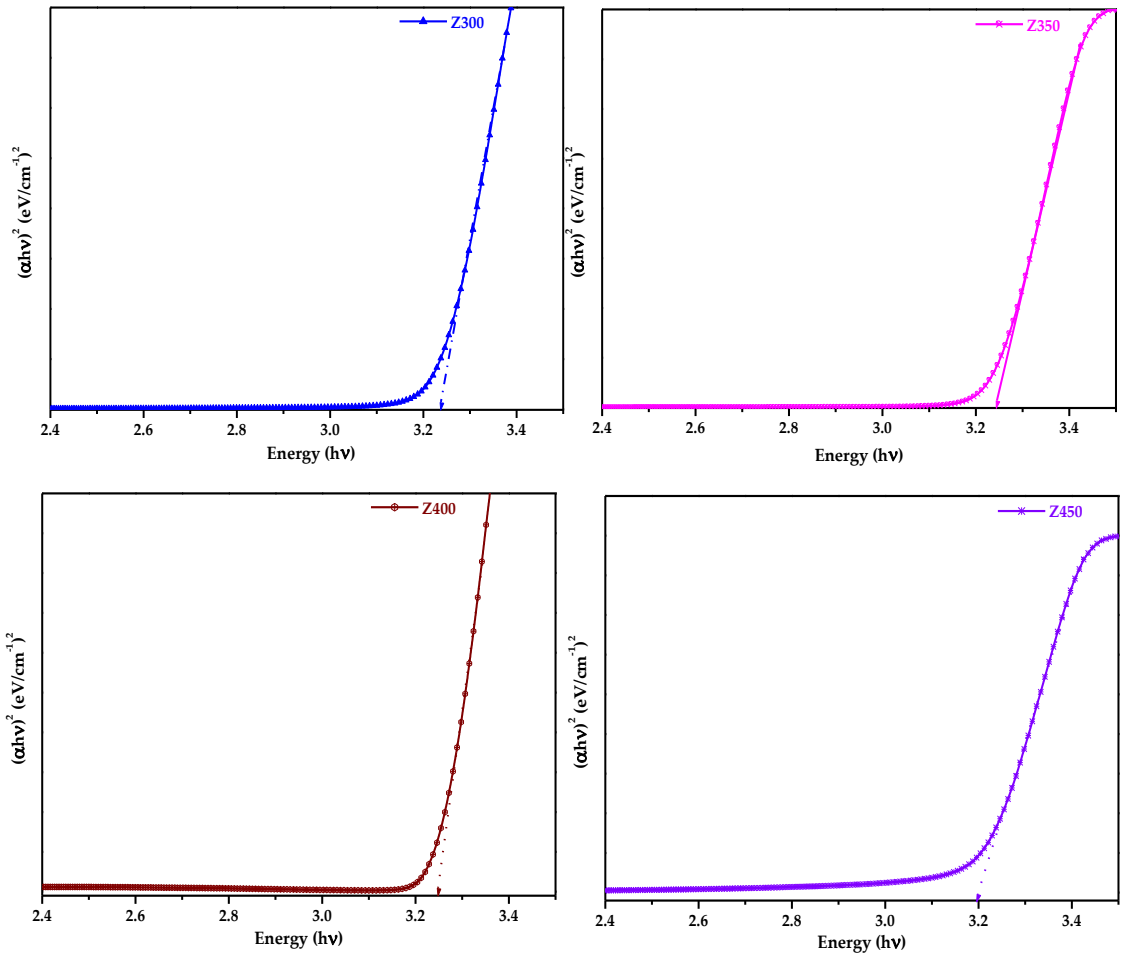

Fig 7. Tauc plot of ZnO film at substrate temperature (a) 300°C (b) 350°C, (c) 400°C and (d) 450°C.

A graph plotted between $(\alpha h\nu)^2$ and $h\nu$ and the optical band gap is derived by extrapolating the linear portion of $(\alpha h\nu)^2$ to$h\nu$. The linearity noticed from the graph represents the direct

transition of band gap of the semiconductor. The band gap of ZnO thin film ranged from 3.24 - 3.19 eV. The film deposited at substrate temperature 450 °C was 3.19 eV. And this trend in band gap may be due to the appearance of band tail from defects and surface roughness [28]. The decrease in the optical band gap as the function of annealing temperature is associated with the interatomic distance [45]. The observed band gap value is in good agreement with the earlier reports [46, 47].

The refractive index (n) was calculated using following equation.

$$n = \frac{1+R}{1-R} + \sqrt{\frac{4R}{(1-R)^2} - k^2}$$

The extinction coefficient is evaluated using the relation

$$k = \frac{\alpha\lambda}{4\pi}$$

The spectral variation in extinction coefficient as a function of wavelength is displayed in the Fig 9.

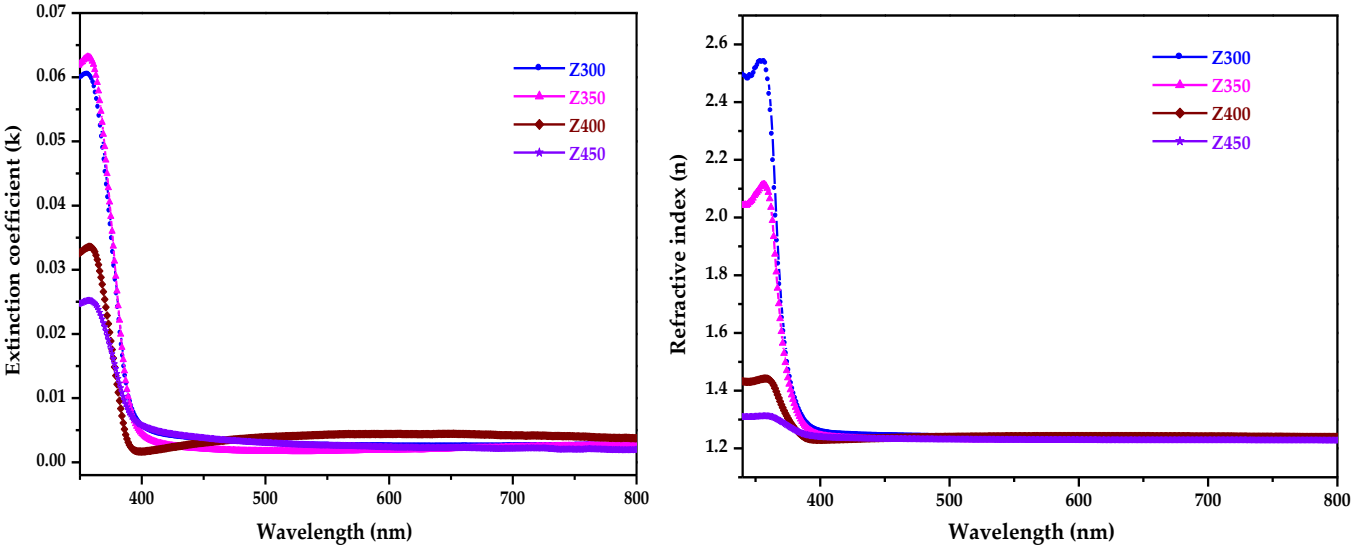

Fig 8. Variation of extinction coefficient and Refractive index with wavelength of ZnO film

The extinction coefficient (*k*) shows decreasing trend with increase in deposition temperature, whereas the ZnO thin film deposited at 400 °C have increasing behavior [34]. From Fig. 8 & 9, the refractive index (n) and extinction coefficient (*k*) decreases with increase in wavelength is observed, is associated with light scattering. The value of refractive index (n) and extinction coefficient (*k*) in visible region is low with that of the theoretical value, accumulating that the ZnO thin film has low dielectric loss [48].

3.6 Photoluminescence Characterization

The room temperature photoluminescence spectra of ZnO film deposited at different substrate temperature is recorded and presented in Fig. 10.

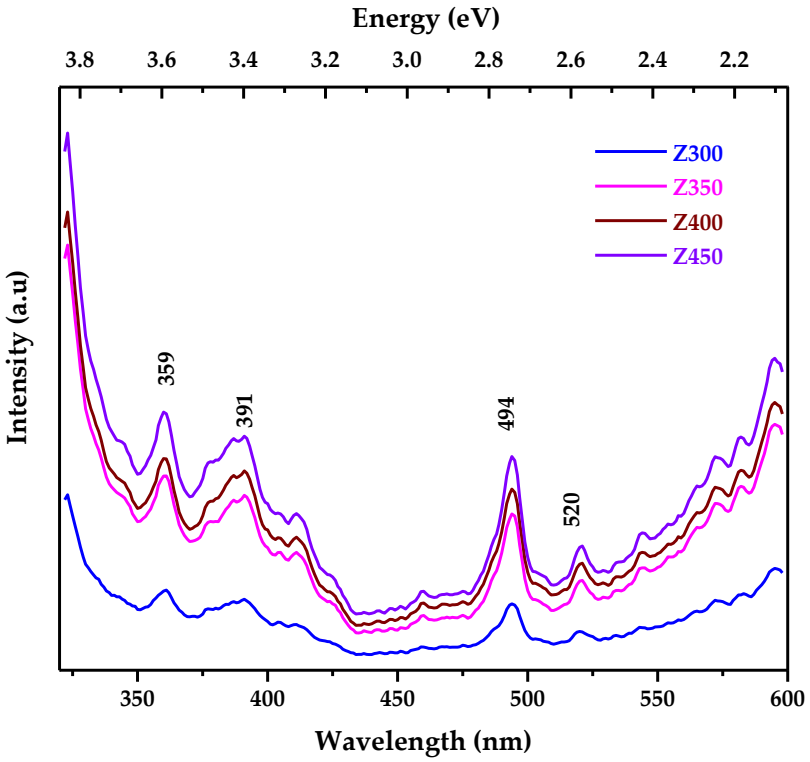

Fig: 10 Room temperature PL spectra of ZnO thin film

The PL spectra of ZnO film were recorded in the wavelength range 300 – 600 nm with excitation wavelength of 320 nm. The different forms of ZnO, such as nano particle, thin film, nano rod, nano sheet etc, manifests two luminescence band, (i) short wavelength band, near the absorption

edge and (ii) long wavelength band, usually in visible green region [49]. As seen from the spectra, ZnO thin film consists of five luminescence peaks at wavelength 360, 390, 411, 494 and 520 nm. The strong peak at 359 nm is due to free exciton (FE) [50] and the 390 nm peak (3.17 eV) corresponds to excitonic emission from near band edge transition of wide band gap of ZnO, i.e, the recombination of excitons through exciton – exciton collision process [51]. The strong band edge transition found to be red shifted compared to the bulk ZnO. This shift is referred to the change in optical band gap of ZnO film [52]. For pure ZnO, defects such as zinc interstitials (Zn_i) and oxygen vacancies (V_o) contributes to PL emission. Also, the emission around 400 – 560 nm wavelength region contains distinct peaks at 411 nm (3.01 eV), 494 nm (2.51 eV) and 520 nm (2.38 eV) originates single/double ionized oxygen vacancy which activate bound magnetic polarons in dilute magnetic semiconductors (DMS) [53, 54]. The violet emission at 411 nm is related to Zn vacancies. The luminescence centered at 494 nm is assigned to as deep level emission (DLE), that arises due to recombination of a photogenerated hole with electron which is the native defects in the surface and sub surface such as oxygen vacancies, Zn interstitials, lattice defects etc., of ZnO [55]. The emission peak 520 nm is due to the transition from conduction band to oxygen antisite level [56]. The strong emission in blue – green region indicates that it could be used in LED application [57].

3.7 Raman characterization

Raman spectroscopy is a powerful non destructive characterization technique for the study of structural properties of oxides. Raman spectra arise from the inelastic scattering of light, mostly in visible region. The ZnO belongs to wurzite structure with C_{6v}^4 symmetry. The representation of brillouin zone is as follows,

$$\Gamma_{op} = 2A_1 + 2B_1 + 2E_1 + 2E_2$$

Where A and B modes presents one fold degeneracy, E modes are twofold degeneracy. For ZnO, there are 12 phonon branches, of which 9 optical and 3 acoustical phonon modes [57]. The Raman spectra of ZnO film is shown in Fig.11.

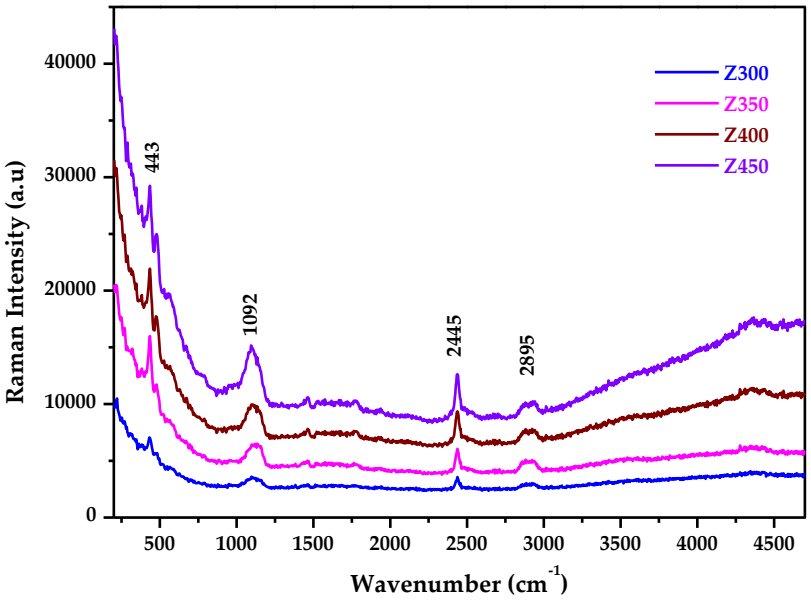

Fig 11. RT Raman Spectra of ZnO thin film

The frequency below 500 cm^{-1} is assigned for transverse acoustical vibrations mode is and the frequency region between 500 and 1300 cm^{-1} related to longitudinal optical modes. For ZnO, B_1 modes are silent and are Raman inactive. The high frequency E_2^{high} mode at 438 cm^{-1} is associated to oxygen atoms, is the characteristics of wurtzite phase [58]. The shift in E_2^{high} peak is observed for the film deposited at 400 °C and 450 °C which account for the intrinsic defect present in the film [59]. The A broad hump around 564 cm^{-1} corresponds to multiple phonon (M) vibration. It is observed that E_1 mode does not appear for ZnO thin film, favoring the growth of ZnO thin film along c- axis. The peak observed at 1110 cm^{-1} and 2890 cm^{-1} corresponds to A1

(2LO) mode and organic residue (CH_3 stretching), (does not decompose completely) respectively [60].

3.8 Magnetic Characterization

The magnetic properties of perfume sprayed ZnO thin film at different substrate temperature 300ºC, 350ºC, 400ºC and 450ºC were measure at room temperature by vibrating sample magnetometer (VSM), Lake shore. The magnetization (M) versus applied magnetic field (H) is displayed in Fig:12

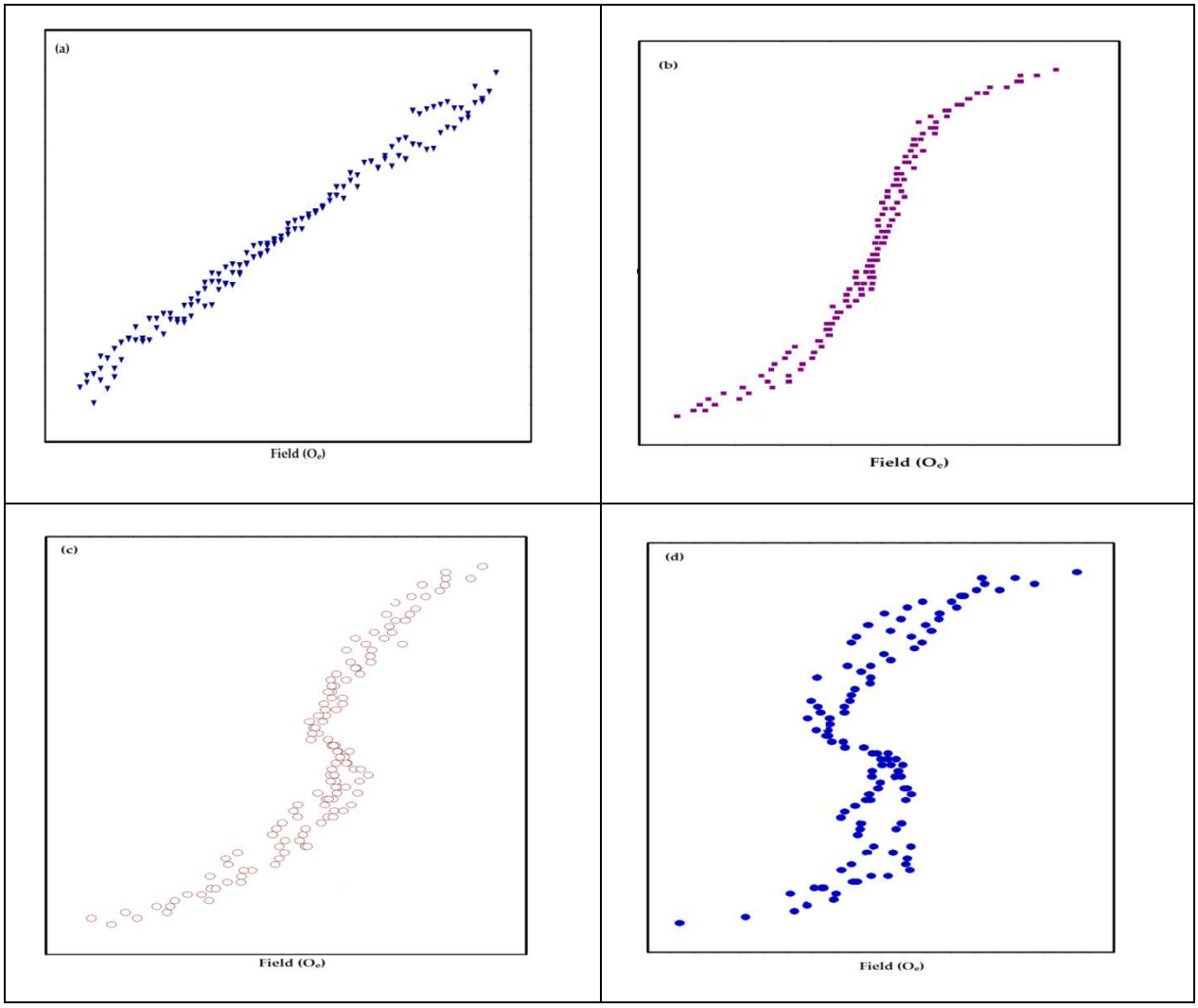

Fig: 12 M – H plot for ZnO thin film at (a) 300ºC, (b) 350ºC, (c) 400ºC and (d) 450ºC

The presence of weak magnetic signal is observed from the Fig and it may be rooted from defects induced in the film [62]. The coercivity (H) increases with substrate temperature and then decreases, while the saturation and remnant magnetization (M_s) decreases. The decrease in saturation magnetization resulted in an increase in coercivity is observed [63]. The ratio $\left[\frac{M_r}{M_s}\right]$ is the measure of squareness (i.e,) square of hysteresis loop. The squareness ratio is relatively close to zero [64,65] and are tabulated in Table:3 .

Table:3 Magnetic properties of ZnO thin film

Samples	Retentivity (emu)	Coercivity (O_e)	Saturation magnetization (M_s)	Squareness ratio $\frac{M_r}{M_s}$	Exchange bias $\frac{H_c}{2}$
Z300	6.98 x 10^{-6}	518	220.6 x 10^{-6}	0.031	259
Z350	4.26 x 10^{-6}	1274	196.8 x 10^{-6}	0.021	637
Z400	0.39 x 10^{-6}	1934	89.5 x 10^{-6}	0.004	967
Z450	3.99x10^{-6}	414	85.1 x 10^{-6}	0.046	207

The bulk ZnO is diamagnetic [66] and in our case the magnetization in ZnO thin film arises due to defects such as cation (Zn) vacancies, preparation methods and microstructure [67,68]. Ferromagnetic behavior observed in metal oxides (pure) is been reported by many researchers [69, 70]. Also, the oxide thin film does not require magnetic cations or oxygen vacancy to become magnetic but the presence of some structural inhomogeneity proceeds to so called intrinsic diluted magnetic semiconductor [61]. The RTFM arises from the intrinsic defects (oxygen vacancy (V_O), zinc vacancies (V_{zn}), Zn clusters), in ZnO that promotes interaction

between localized spins and bound magnetic polarons (BMP) (two polarons separated by small distance is smaller than the diameter of the polaron) [71] which may lead to application in spintronic and high density magnetic storage devices. The observed RTFM behavior in DMS is attributed to the oxygen vacancies. As the substrate temperature increases, the unconventional shape in magnetic loop is observed in Fig.12 (c & d), i.e, changed from ferromagnetic to diamagnetic state [72].

4. Conclusion

The wurtzite ZnO thin film deposited on glass substrate using perfume atomizer. The structural and micro structural, morphological, optical and photoluminescence property of ZnO thin film were studied. The XRD patterns reveal preferred orientation along (1 0 1) plane upto 400ºC and above 400ºC reorientation of planes are observed. Well defined grains with boundaries and wrinkle shaped nanofibers are examined from FESEM as well as roughness of ZnO thin film revealed from AFM. The low and high surface roughness is observed for the film at 300ºC and 450ºC respectively. The ZnO film at 450ºC could be used as gas sensors owing to its roughness. The ZnO thin film exhibits transmittance of > 80% which is preferred for optoelectronic and solar cell devices. The optical bandgap energy ranges from 3.24 to 3.19eV. The green emission peak of ZnO thin film is adaptable for LED applications. Different phonon modes are obtained from Raman analysis. The intrinsic exchange interaction arising from defects such as oxygen vacancies, zinc vacancy assists BMP and is responsible for room temperature ferromagnetism in ZnO thin film.

Conflict of Interest: On behalf of all authors, the corresponding author states that there is no conflict of interest.

Funding: Not applicable

References

1. C. Jinkai, X. He, W. Wang, W. Xuan, J. Zhou, X. Wang, S R. Dong, S. Garner, P. Cimo, J K. Luo, Mater Chem C. **2**, 9109–9114 (2014).
2. J.Wojnarowicz, R. Mukhovskyi, E. Pietrzykowska, S. Kusnieruk, J. Mizeracki, W. Lojkowski, Beilstein J Nanotechnol **7**, 721–732 (2016).
3. RM. Mohite, RR. Kothawale, Indian J Chem. **54**A, 872-876 (2015)
4. H. Li, X. Li, W. Dong, J .Xi, X Wu, Appl Phys A. **124**, 412 (2018).
5. J. Lv, Z. Yang, C. Wang, S. Wang, Y. Ma, G. Zhou, J. Jiang, Q. Zhu, M. Zhao, X. Chen Appl Phys A. **126**, 290 (2020).
6. A. R. Nimbalkar, M. G Patil, Physica B. **527**, 7–15 (2017).
7. K. Verma, B. Chaudhary, V. Kumar, V. Sharma, M. Kumar, Vacuum. **146**, 524-529 (2017).
8. B. Kadem, HA. Banimuslem, A. Hassan, Karbala International Journal of Modern Science. **3**, 103-110 (2017).
9. T. Srinivasulu, K. Saritha, K.R. Reddy, Mod Electron Mater. **3**,76–85 (2017).
10. T. Long, S. Yin, K. Takabatake, P. Zhnag, T. Sato, Nanoscale Res Lett. **4**, 247–253 (2009).
11. L. Znaidi, G S. Illia, S. Benyahia, C. Sanchez, A V. Kanaev, Thin Solid Films. **428**, 257-262 (2003).
12. A A. Ahmad, A M. Alsaad, Q M. Al-Bataineh, M A. Al-Naafa, Appl Phys A. **124**, 458 (2018).
13. A M. Alsaad, A A.Ahmad, I A. Qattan, Q M. Al-Bataineh, Z. Albataineh, Crystals. **10**, 252 (2020).
14. A. López-Suárez, D. Acosta, C. Magaña, F. Hernández, J Mater Sci - Mater Electron. **31**, 7389–7397 (2020).

15. K. Ravichandran, A J. Santhosam, M. Sridharan, Surf Interfaces. **18**, 1004122 (2020).
16. G. Ojeda-Barrero, A I. Oliva-Avilés, A I. R D. Oliva, Maldonado, M. Acosta, G M. Alonzo-Medina, Mater Sci Semicond Process. **79**, 76 (2018).
17. S A. Kamaruddin, K Y. Chan, H K.Yow, M Z. Sahdan, H. Saim, D. Knipp, Appl Phys A. **104**, 263–268 (2011).
18. U. Manzoor, M. Islam, L. Tabassam, SU. Rahman, Physica E. **41**, 1669–1672 (2009).
19. S. Hamrouni, MS.AlKhalifah, MS. El-Bana, SK. Zobaidi, S. Belgacem, Appl Phys A. **124**,555 (2018).
20. V. Ghafouri, A. Ebrahimzad, M. Shariati, Scientia Iranica. **20**(3), 1039-1048 (2013).
21. MT. Hosseinnejad, M. Shirazi, M. Ghoranneviss, MR. Hantehzadeh, E. Darabi, Journal of Inorganic and Organometallic Polymers and Materials.**26**(2),405-12 (2016).
22. H. Sutanto, S. Durri, S. Wibowo, H. Hadiyanto, E. Hidayanto, Physics Research International. **2016**, (2016).
23. E. Muchuweni, TS. Sathiaraj, H. Nyakotyo, Heliyon. **3**(4), e00285 (2017).
24. M. M. H.Farooqi, R. K. Srivastava, Proceedings of the National Academy of Sciences, India Section A: Physical Sciences. 1-15 (2019).
25. KM. Kang, Y. Wang, M. Kim, HH. Park, Thin Solid Films. **660**, 913-919 (2018).
26. CY. Tsay, KC. Pai, Thin Solid Films. **654**, 11-15 (2018).
27. N. Kumari, SR. Patel, JV. Gohel, Opt Quant Electron. **50**, 1-22 (2018).
28. K. Sadananda, KV. Bangera, GK. Shivakumar, Appl Nanosci. **4**,209–216 (2014).
29. AH. Hammad, MS. Abdel-Wahab, S. Vattamkandathil, AR. Ansari, Phys B. **540**, 1-8 (2018).
30. O. Dimitrov, D. Nesheva, V. Blaskov, I. Stambolova, S. Vassilev, Z. Levi, V. Tonchev, Mater Chem Phys. **148**, 712 – 719 (2014).

31. M. Shahjahan, MK. Khan, MF. Hossain, S.Biswas, T.Takahashi, J. Vac Sci Technol A. **27**(4), 885-888 (2009).
32. L. Znaidi, T. Touam, D. Vrel, N. Souded, S. Ben Yahia, O. Brinza, A. Fischer, A. Boudrioua, Acta Phys Pol A. **121**, 165-168 (2012).
33. A. Sharmin, S. Tabassum, MS. Bashar, ZH. Mahmood, Journal of Theoretical and Applied Physics. **13**,123-132 (2019).
34. MH. Kabir, MM. Ali, MA. Kaiyum, MS. Rahman, Journal of Physics Communications. **3**(10), 105007 (2019).
35. MR. Prasad, M. Haris, M. Sridharan, J Mater Sci: Mater Electron. **28**, 11367–11373 (2017).
36. H. Bahadur, AK. Srivastava, RK. Sharma, S. Chandra, Nanoscale Res Lett. **2**, 469–475 (2007).
37. NF. Ahmad, K. Yasui, AM. Hashim, Nanoscale Res Lett. **10**, 1-9 (2015).
38. MR. Prasad, M. Haris, M. Sridharan, Sens Actuators A. **269**, 435–443 (2018).
39. U. Chaitra, MG. Mahesha, D. Kekuda, KM. Rao, Appl Phys A. **125**, 394 (2019).
40. S. Talam, SR. Karumuri, N. Gunnam, Synthesis, ISRN Nanotechnology. **2012**, (2012).
41. H. Zaka, B. Parditka, Z. Erdélyi, HE. Atyia, P. Sharma, SS. Fouad, Optik. **203**,163933 (2020).
42. I. Soumahoro, G. Schmerber, A. Douayar, Colis S, M. Abd-Lefdil, N. Hassanain, A. Berrada, D. Muller, A. Slaoui, H. Rinnert, A. Dinia, J Appl Phys. **109**, 033708 (2011).
43. L. Brus, J Phys Chem B. **90**, 2555 (1986).
44. NS. Pesika, KJ. Stebe, PC. Searson, J Phys Chem B. **107**, 10412 (2003).
45. D. Komaraiah, E. Radha, Y. Vijayakumar, J. Sivakumar, MR. Reddy, R. Sayanna, Modern Research in Catalysis. **5**(4),130-146 (2016).

46. KM. Sandeep, S. Bhat, SM. Dharmaprakash, J Phys Chem Solids **104**, 36-44 (2017).

47. N. Srinatha, P. Raghu, HM. Mahesh, B. Angadi, J Alloys Compd. **722**, 888-895 (2017).

48. A. Bedia, FZ. Bedia, M. Aillerie, N. Maloufi, B. Benyoucef, Energy Procedia. **50**,603-609 (2014).

49. AK. Ghosh, KK. Som, S. Chatterjee, BK. Chaudhuri, Phys Rev B. **51**, 4842–4848 (1995).

50. SS. Hussain, H. Noor, S. Riaz, A. Hashmi, S. Naseem, In ACEM16) The 2016 World Congress on Advances in Civil, Environmental, and Materials Research, Korea on August (Vol. 28) (2016).

51. Y. Li, HQ. Wang, H. Zhou, D. Du, W. Geng, D. Lin, X. Chen, H. Zhan, Y. Zhou, J. Kang, Nanoscale Res Lett. **12**, 551(2017).

52. PA. Rodnyi, IV. Khodyuk, Optics and Spectroscopy. **111**(5), 776-785 (2011).

53. J. Kazmi, PC. Ooi, B.T. Goh, MK. Lee, MM. Wee, SS. Karim, SR. Raza, MA. Mohamed, RSC Adv. **10**, 23297-23311(2020).

54. AK. Rana, Y. Kumar, P. Rajput, SN. Jha, D. Bhattacharyya, PM. Shirage, ACS Applied Materials & Interfaces. **9**, 7691-7700, (2017).

55. H. Liu, X. Wang, M. Li, S. Yu, R. Zheng, Ceram Int. **45**, 14347–14353 (2019).

56. AS. Gadallah, MM. El-Nahass, Advances in Condensed Matter Physics. 2013 (2013).

57. M. Xin, LZ. Hu, DP. Liu, NS. Yu, Superlattices and Microstructures. **74**, 234–241 (2014).

58. V. Russo, M. Ghidelli, P. Gondoni, CS. Casari, A. Li Bassi, J Appl Phys. **115**, 073508 (2014).

59. G. Srinivasan, N. Gopalakrishnan, YS. Yu, R. Kesavamoorthy, J. Kumar, Superlattices and Microstructures. **43**(2),112-119 (2008).

60. E. Nowak, M. Szybowicz, A. Stachowiak, W. Koczorowski, D. Schulz, K. Paprocki, K. Fabisiak, S. Los, Applied Physics A. **126**(7),1-12 (2020).
61. M. Schumm, ZnO- based semiconductors studied by Raman spectroscopy: semimagnetic alloying, doping and nanostructures. Phd thesis (2008).
62. DC. Agarwal, UB. Singh, S. Gupta, R. Singhal, PK. Kulriya, F. Singh, A. Tripathi, J. Singh, US. Joshi, DK. Avasthi, Scientific reports. **9**, 1-12 (2019).
63. ZN. Kayani, A. Usman, H. Nazli, R. Sagheer, S. Riaz, S. Naseem, Applied Physics A. **126**, 559 (2020).
64. S. Kumar, A. Sharma, M. Singh, SP. Sharma, Archives of Physics Research. **5**, 18-24 (2014).
65. K. Praveena, K. Sadhana, HS. Virk, Solid State Phenomena Series, Trans Tech Publications Ltd. **232**, 45-64 (2015).
66. NF. Mott, Philos. Mag. **19**, 835–852(1969).
67. Q. Wang, Q. Sun, G. Chen, Y. Kawazoe, P. Jena, Phys. Rev. B **77,** 205411(2008).
68. M. Kapilashrami, J. Xu, V. Ström, KV. Rao, L. Belova, Applied Physics Letters. **95**, 033104 (2009).
69. S. Kumar, YJ. Kim, BH. Koo, S. Gautam, KH. Chae, R. Kumar, CG. Lee, Materials Letters. **63**(2),194-6 (2009).
70. Z. Yan, Y. Ma, D. Wang, J. Wang, Z. Gao, L. Wang, P. Yu, T. Song, Applied physics letters. **92**(8),081911. (2008).
71. N. Ali, AR. Vijaya, ZA. Khan, K. Tarafder, A. Kumar, MK. Wadhwa, B. Singh, S. Ghosh Scientific reports. **9**, 1-3 (2019).

72. D. Aryanto, C. Kurniawan, A. Subhan, T. Sudiro, P. Sebayang, M. Ginting, SM. Siregar, MN. Nasruddin, IOP Conference Series: Materials Science and Engineering. 202, 012049 (2017).

Figures

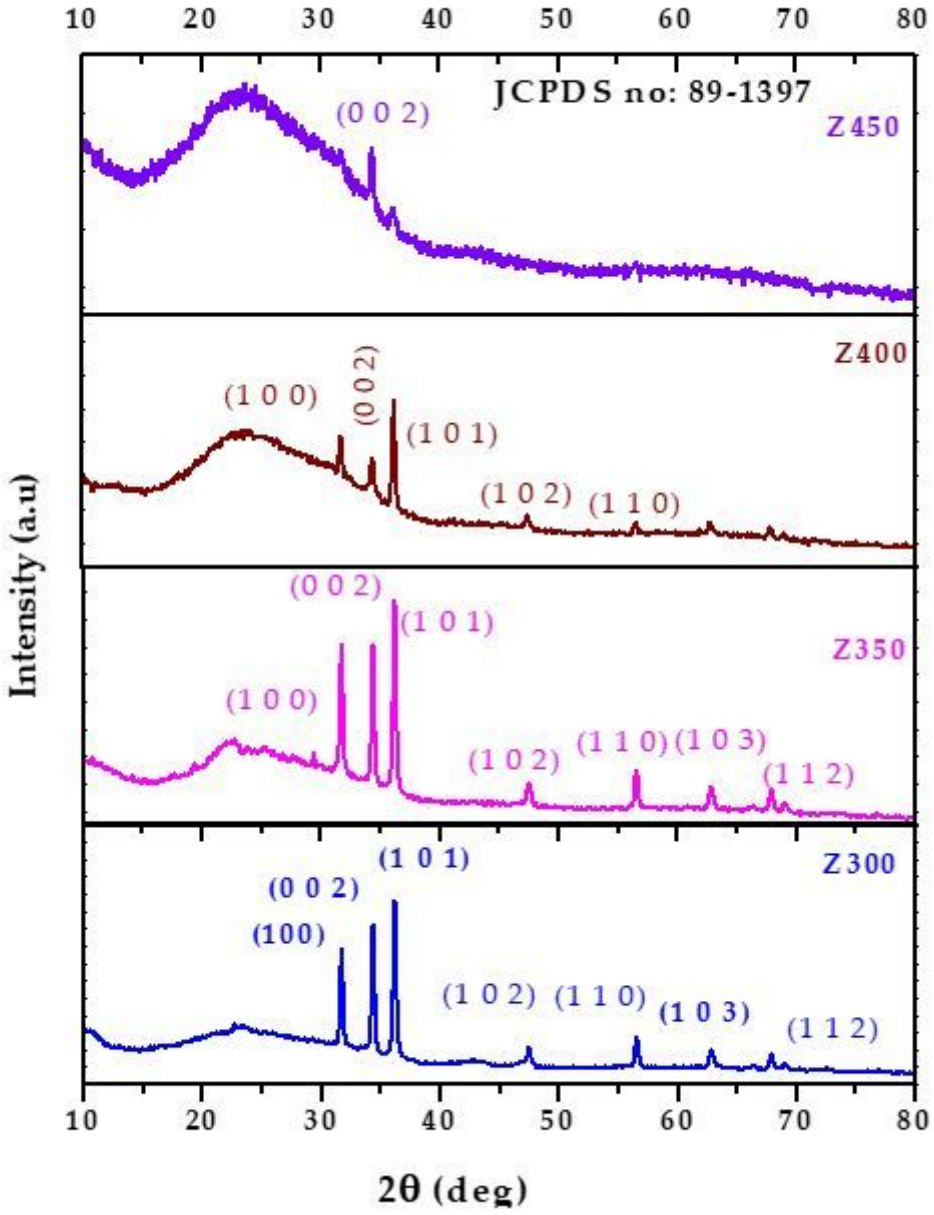

Figure 1

XRD patterns of annealed ZnO thin film at different substrate temperature

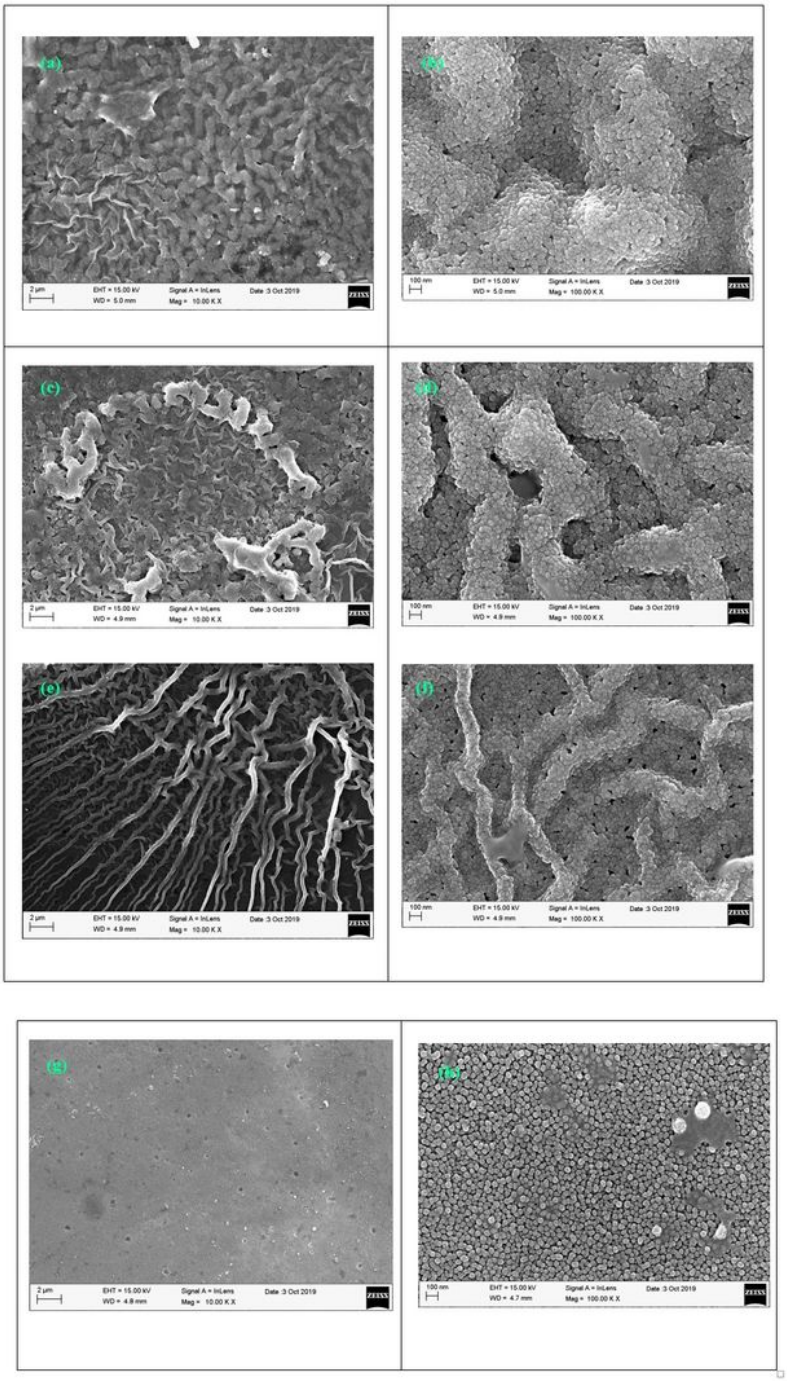

Figure 2

FE-SEM images of ZnO thin films at substrate temperature (a,b) 300°C, (c,d) 350°C, (e,f) 400°C and (g,h) 450°C

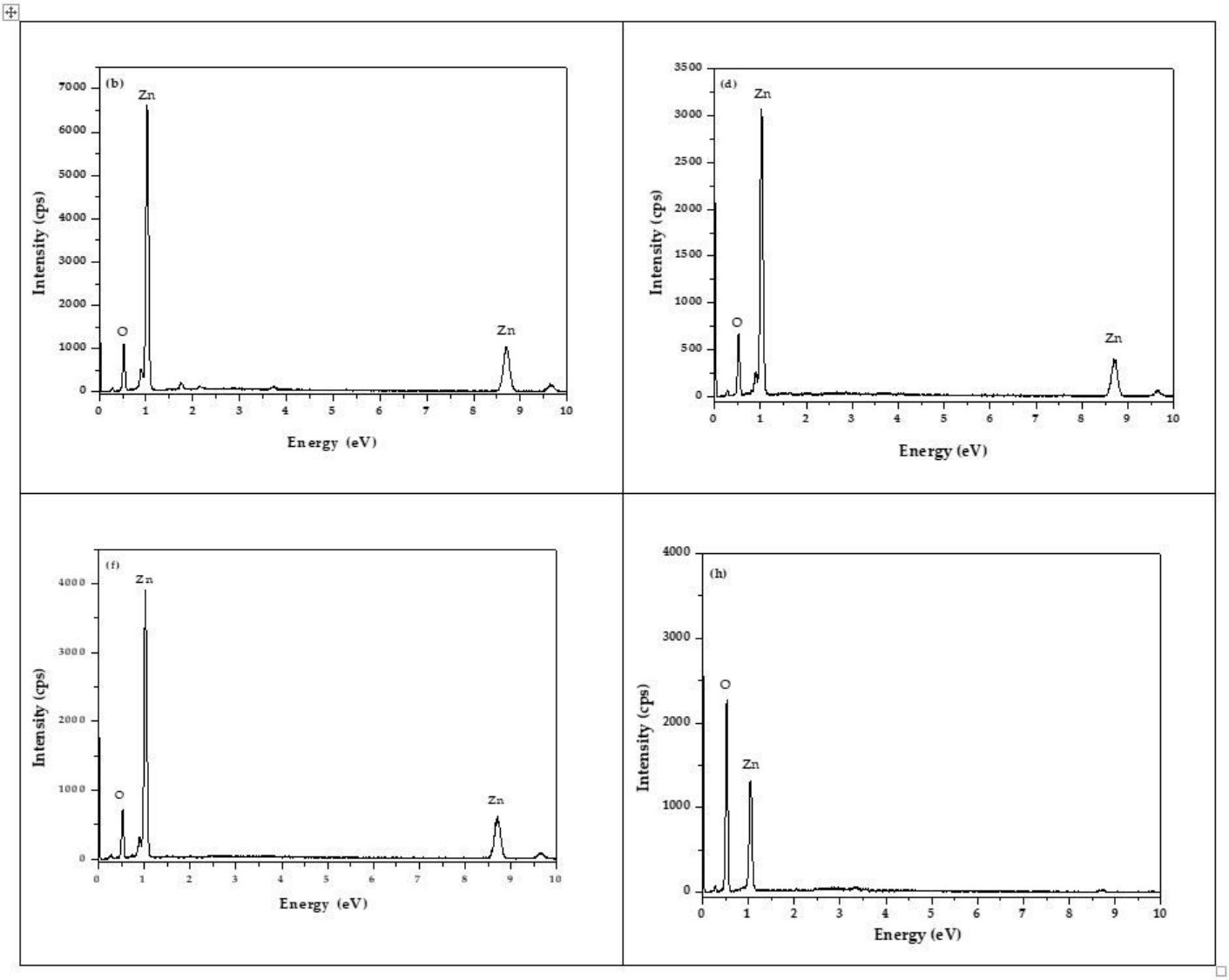

Figure 3

EDS spectra of ZnO film at substrate temperatures

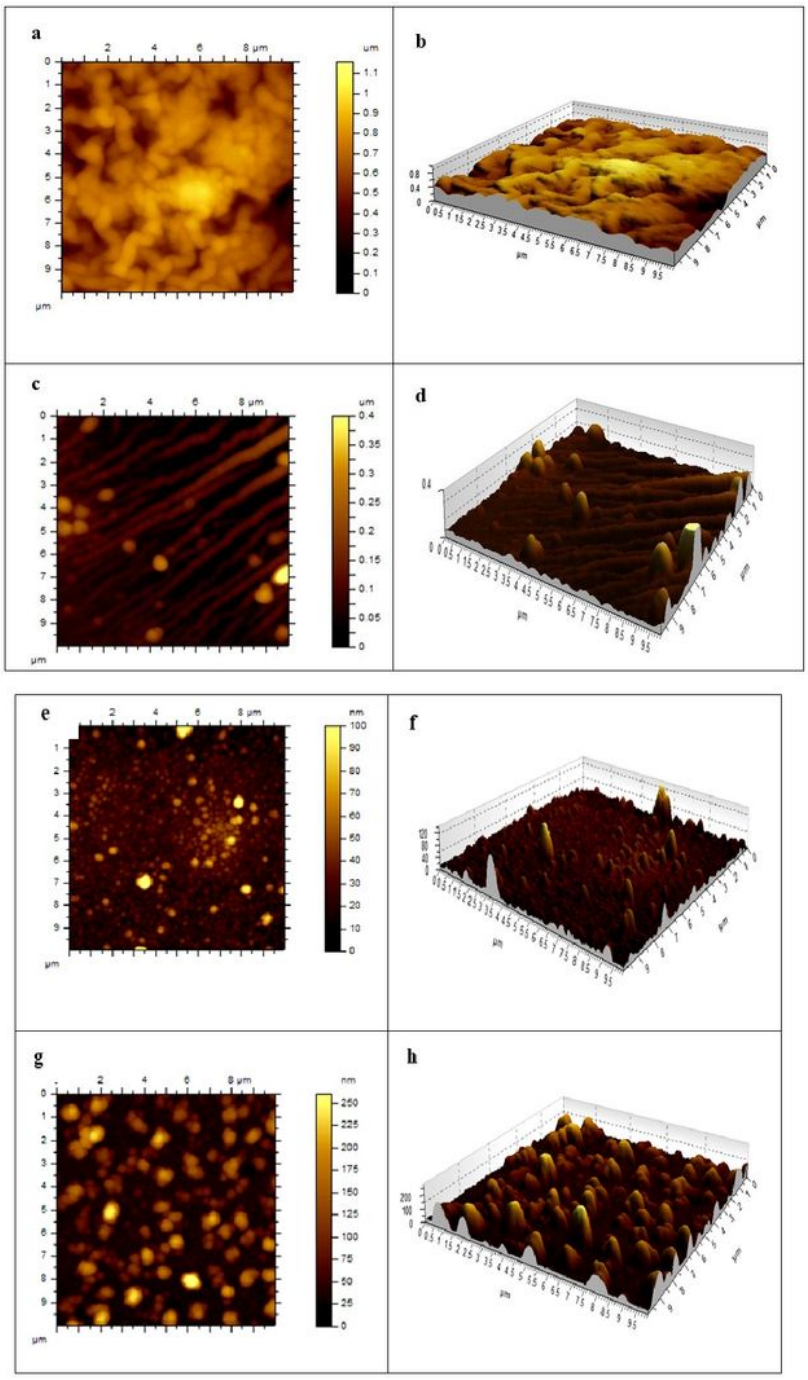

Figure 4

(a - h), 2D and 3D AFM image of ZnO thin film at different substrate temperatures.

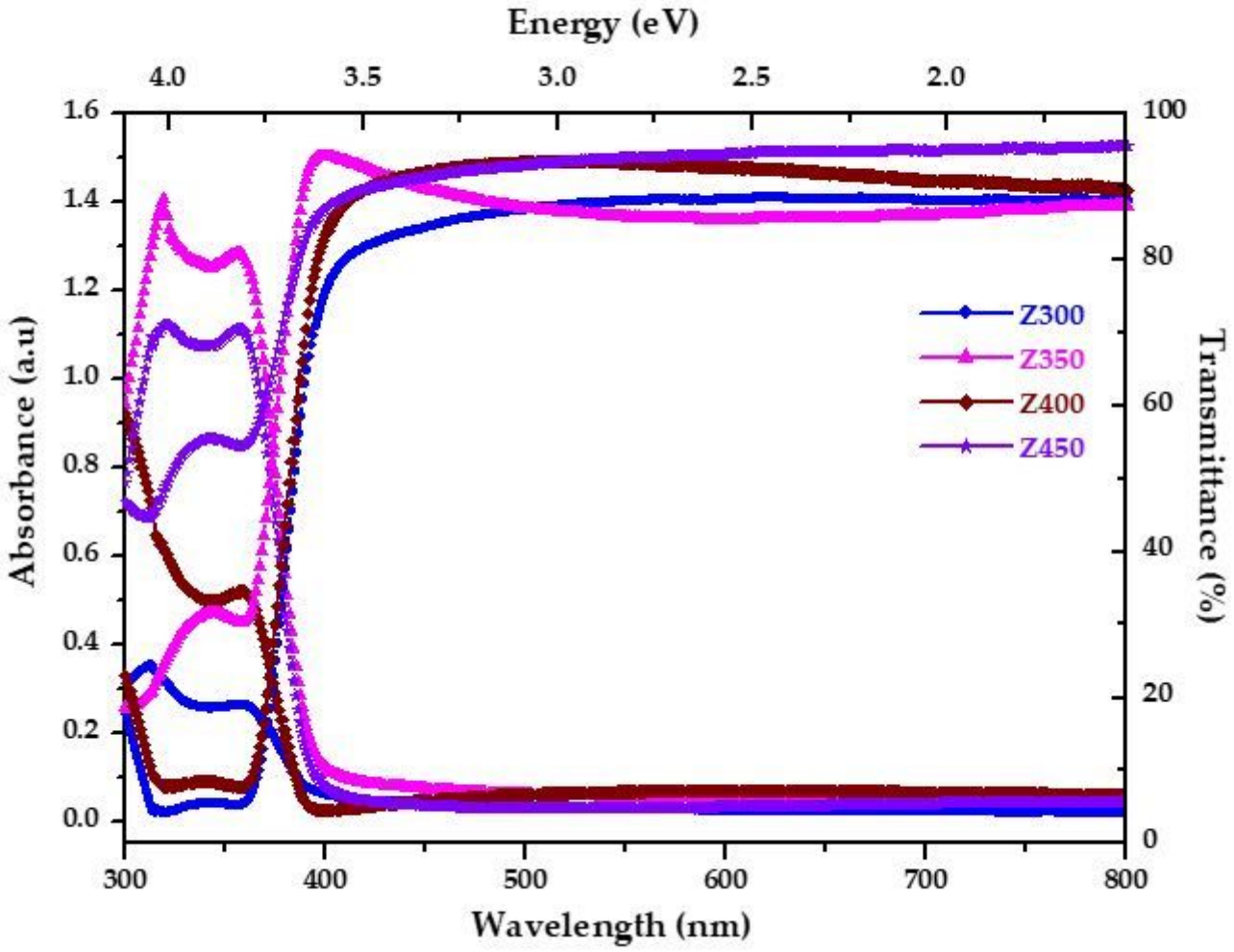

Figure 5

UV Vis absorbance and transmittance spectra of ZnO thin film

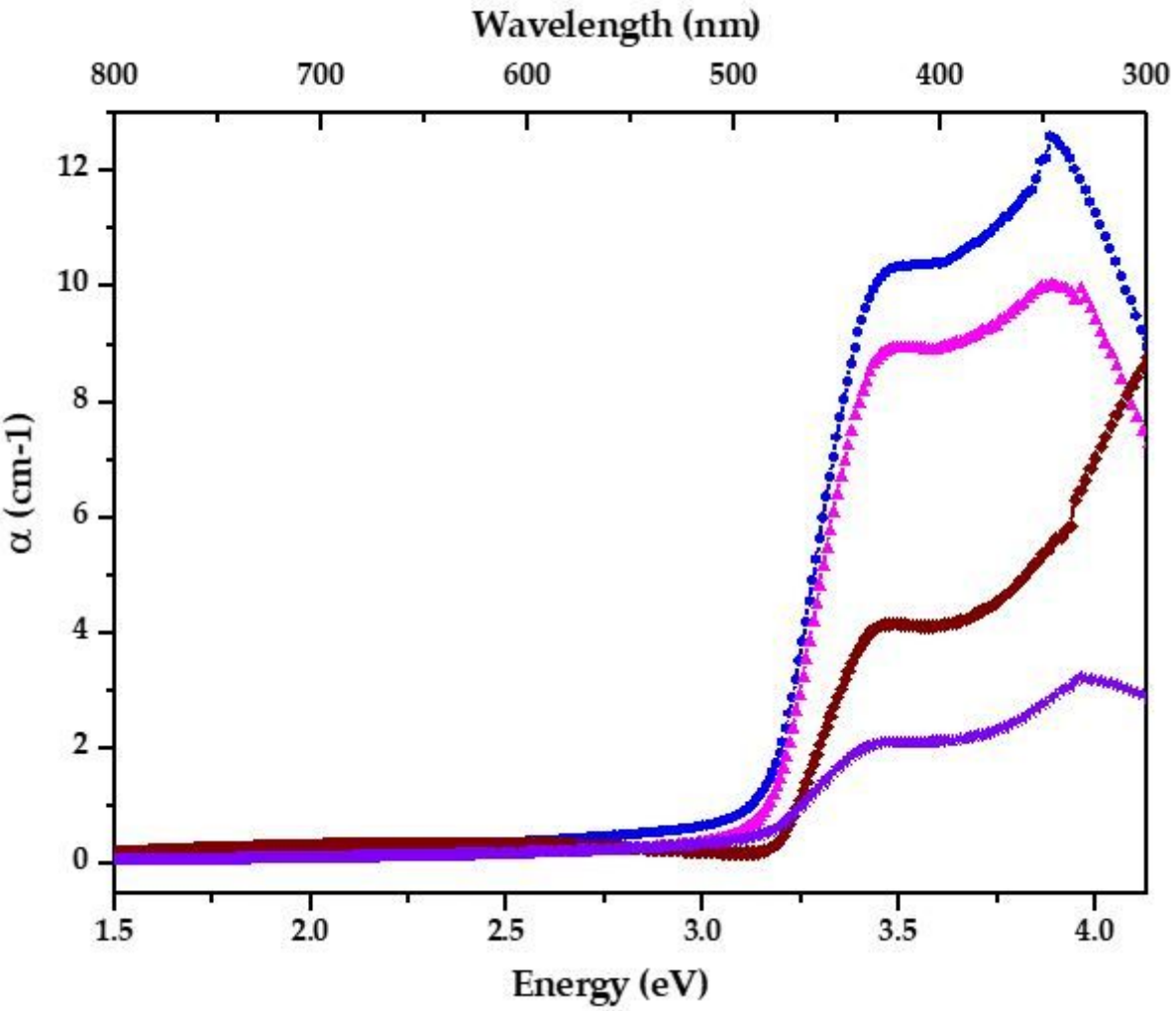

Figure 6

Absorption coefficient Vs Wavelength plot of ZnO film

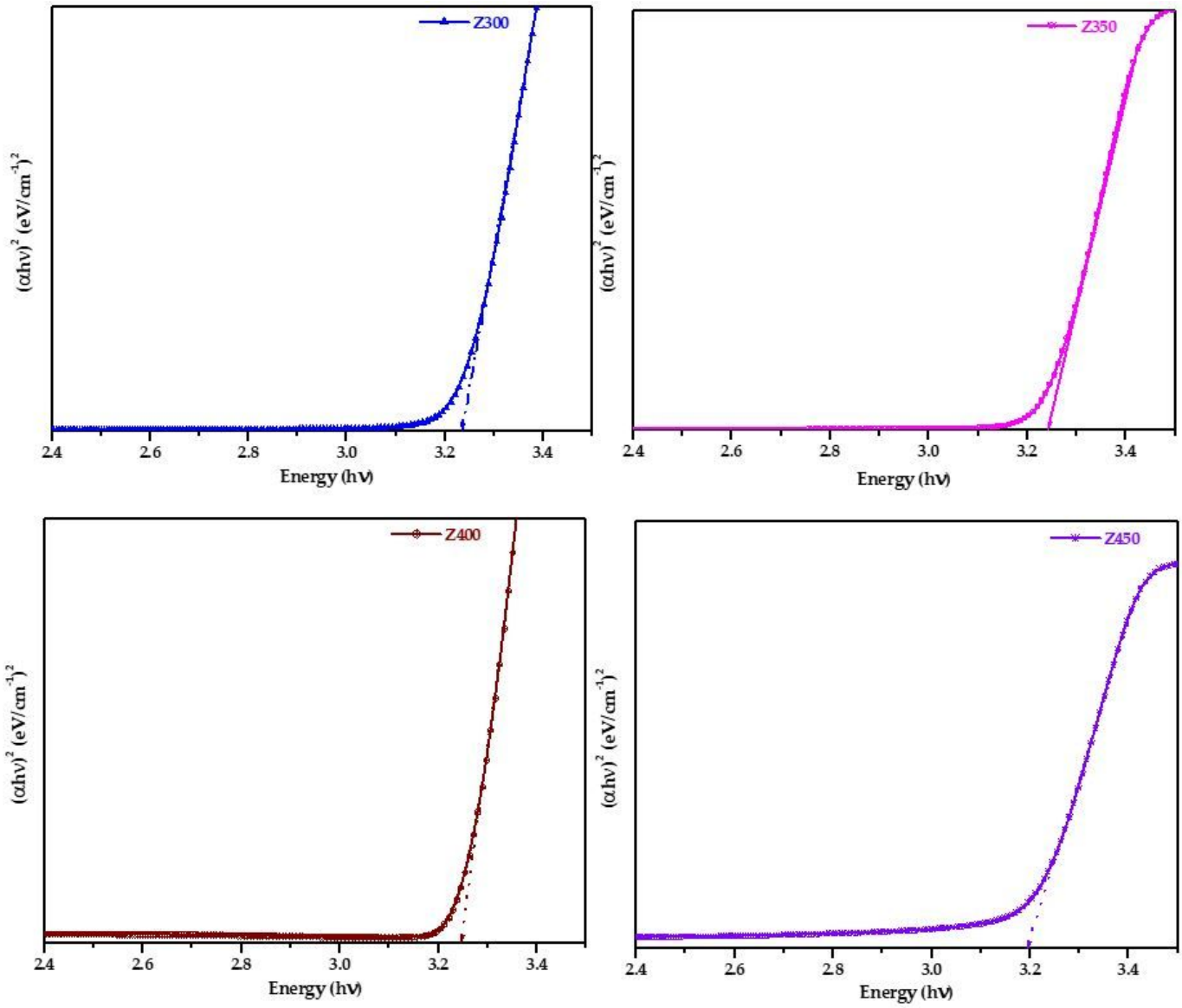

Figure 7

Tauc plot of ZnO film at substrate temperature (a) 300°C (b) 350°C, (c) 400°C and (d) 450°C.

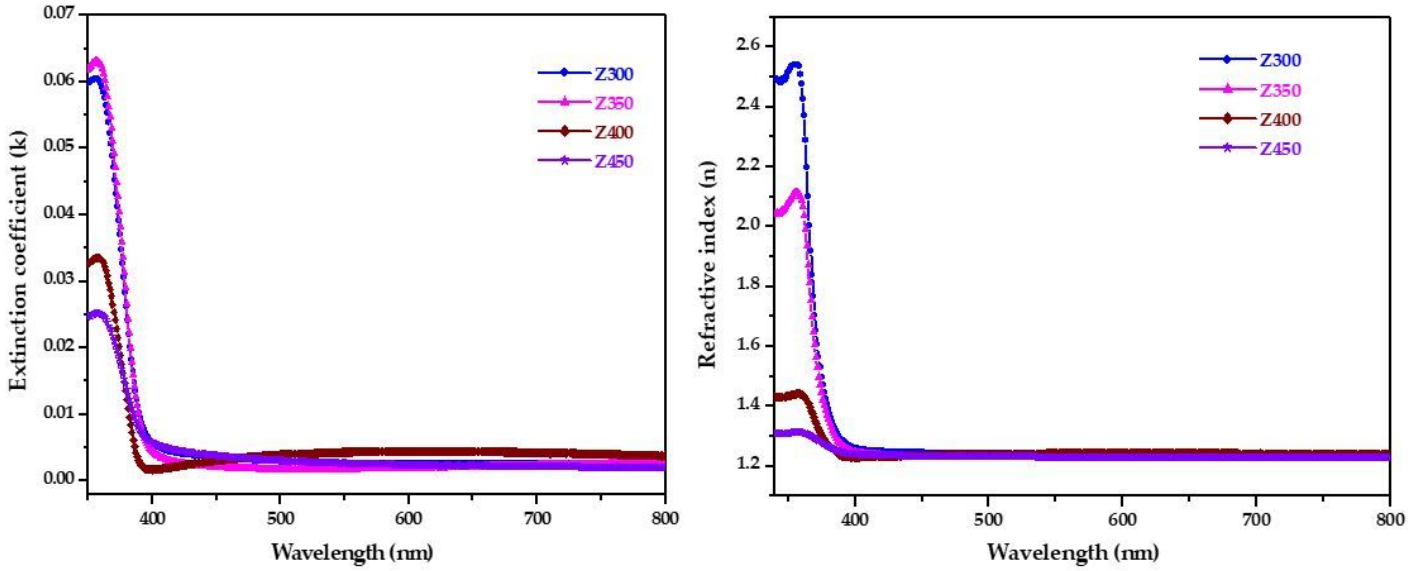

Figure 8

Variation of extinction coefficient and Refractive index with wavelength of ZnO film

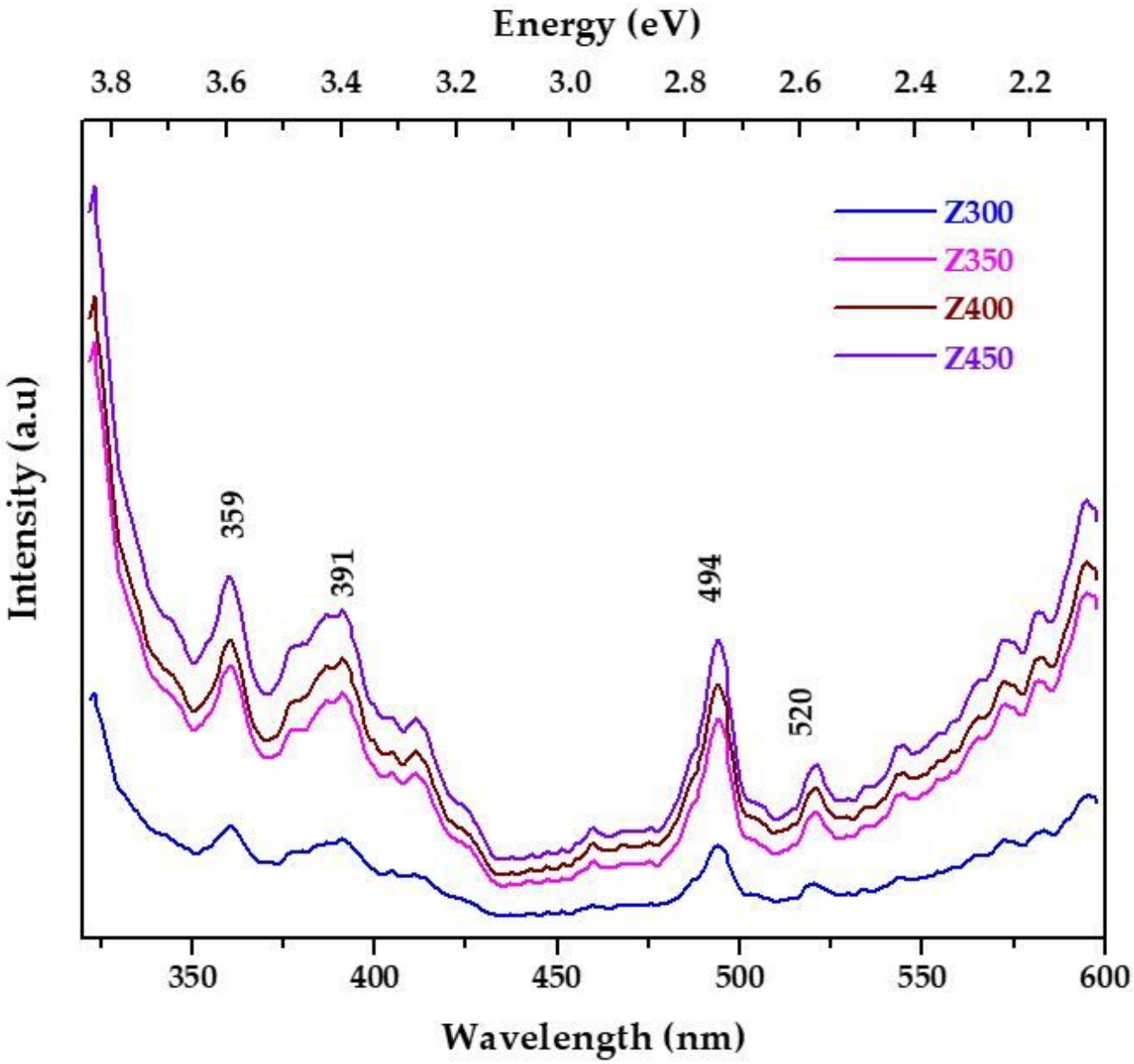

Figure 9

Room temperature PL spectra of ZnO thin film

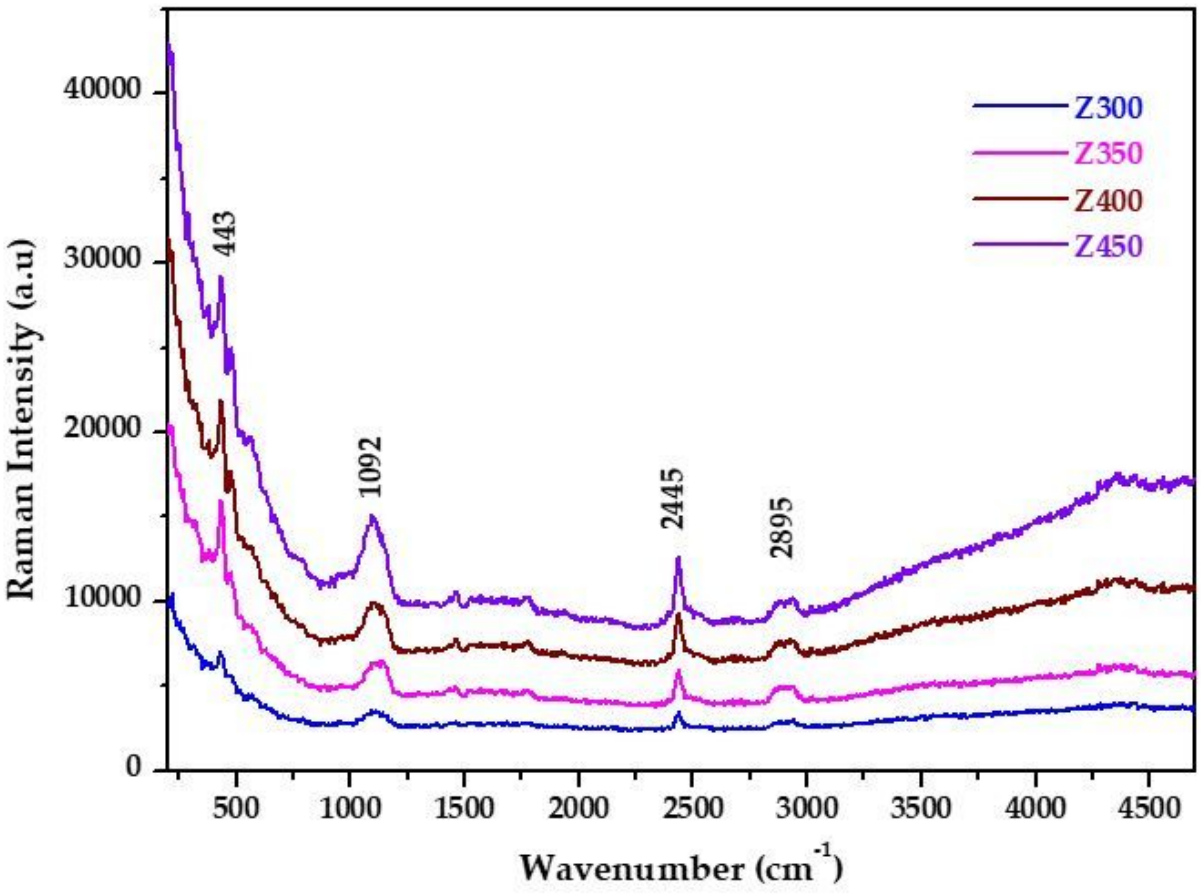

Figure 10

RT Raman Spectra of ZnO thin film

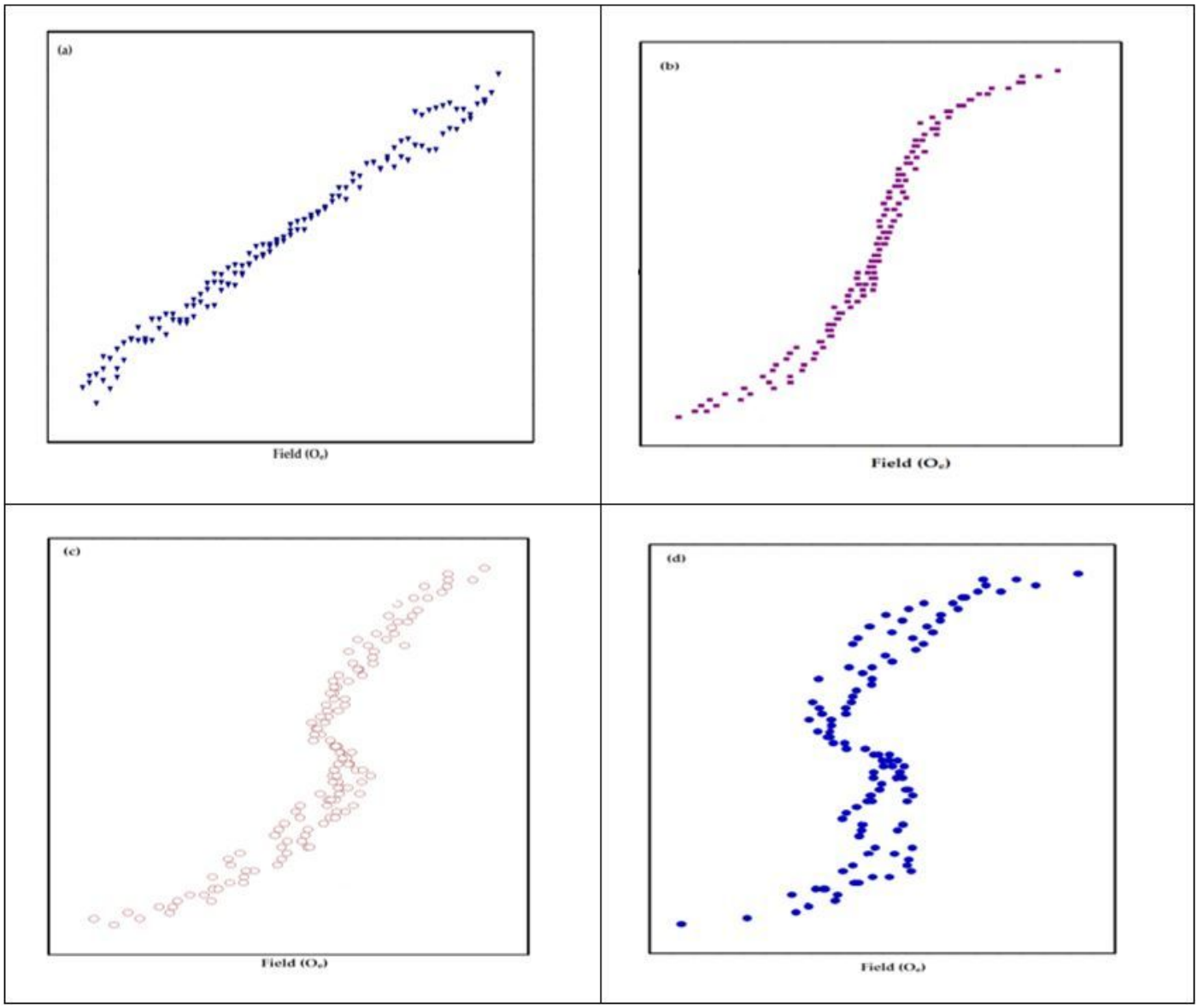

Figure 11

M – H plot for ZnO thin film at (a) 300°C, (b) 350°C, (c) 400°C and (d) 450°C